Cao *et al.*
Natural Products and Bioprospecting (2024) 14:61
https://doi.org/10.1007/s13659-024-00481-9

Natural Products and Bioprospecting

ORIGINAL ARTICLE

Discovery of structurally diverse sesquiterpenoids from *Streptomyces fulvorobeus* isolated from *Elephas maximus* feces and their antifungal activities

Lu Cao[1], Jun-Feng Tan[1], Zeng-Guang Zhang[1], Jun-Wei Yang[1], Yu Mu[1], Zhi-Long Zhao[2], Yi Jiang[3*], Xue-Shi Huang[1*] and Li Han[1*]

Abstract

Thirty-six structurally diverse sesquiterpenoids, including caryolanes (**1–12**), germacranes (**13–16**), isodaucane (**17**), cadinanes (**18–22**), epicubenols (**23**, **24**), oplopanane (**25**), pallenanes (**26**, **27**), and eudesmanes (**28–36**), were isolated from the fermentation broth of *Streptomyces fulvorobeus* derived from *Elephas maximus* feces. Pallenane is a kind of rarely reported sesquiterpene with a distinctive C5/C3 bicyclic skeleton and was firstly found from microbial source. The structures of fifteen new compounds (**1–4**, **13–15**, **17**, **18**, **22**, **23**, **25–28**) were established through detailed spectroscopic data analysis, which included data from experimental and calculated ECD spectra as well as Mosher's reagent derivative method. Compound **34** exhibited moderate antifungal activity against *Cryptococcus neoformans* and *Cryptococcus gattii* with MIC values of 50 μg/mL. It effectively inhibited biofilm formation and destroyed the preformed biofilm, as well as hindered the adhesion of *Cryptococcus* species. The current work would enrich the chemical diversity of sesquiterpenoid family.

Keywords Sesquiterpenoids, *Streptomyces fulvorobeus*, Fermentation, Antifungal activity

*Correspondence:
Yi Jiang
jiangyi@ynu.edu.cn
Xue-Shi Huang
huangxs@mail.neu.edu.cn
Li Han
hanli@mail.neu.edu.cn
Full list of author information is available at the end of the article

Graphical Abstract

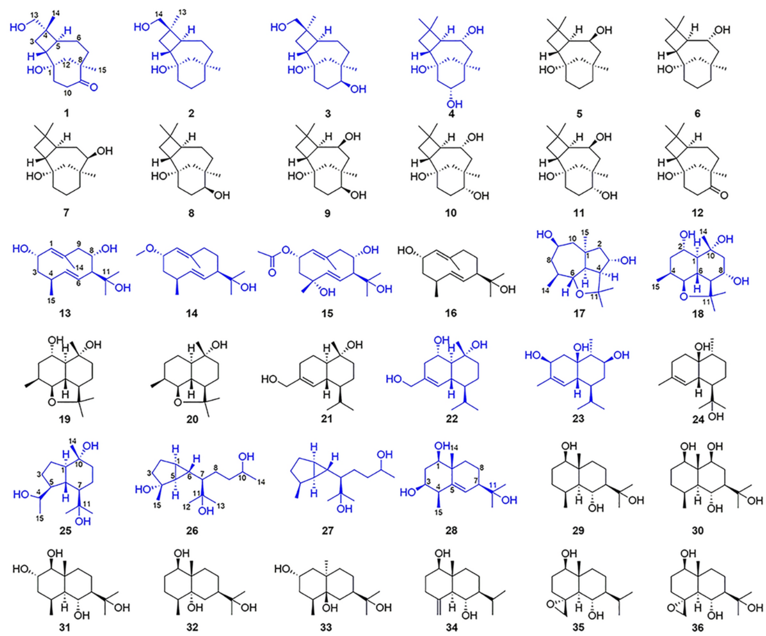

Streptomyces fulvorobeus

- Structurally diverse sesquiterpenoids including 15 new sesquiterpenoids
- **34** against *Cryptococcus* species with MIC values of 50 μg/mL
- Inhibited biofilm formation and destroyed the preformed biofilm
- Exerted a restraining effect on the adherence of *Cryptococcus* species

1 Introduction

A huge amount of microorganisms colonize the guts of mammals [1, 2]. These microbes and their metabolites possess the ability to regulate intestinal epithelial cell proliferation, angiogenesis, host energy, lipid metabolism, and inflammatory immune response [3–6]. The bacterial community in fresh and unpolluted feces could largely represent the distal gut bacteria. Due to its noninvasive and convenient collection, fecal samples are commonly used for studying gut bacteria [7, 8]. In the past few years, the authors have reported on research regarding the structural diversity, antimicrobial, anti-inflammatory, and cytotoxic activities associated with animal feces [9–15]. These findings demonstrated that animal gut microorganisms could be considered as an abundant and significant microbial resource, which has prompted an investigation into the secondary metabolites produced by actinobacteria inhabiting in the animal intestinal tract.

Sesquiterpenoids undergo diverse cyclization cascades with their substrate farnesyl diphosphate (FPP), resulting in a variety of structural skeleton types and are widely distributed in plants, fungi, and red algae [16–18]. However, the discovery of these metabolites in bacteria has been limited due to difficulties in separation, low yield, and the absence of chromophores [19, 20]. With further research, the genome mining technology was applied and it has been found that terpene synthase and cyclase are also widely distributed in bacteria, especially actinomycetes [20–22]. According to the literatures, germacrane, pentalenene, zizaane, cadinane, and caryolane are the five most commonly detected type of sesquiterpenoids in bacteria [21, 23]. The exploration of a wider range of sesquiterpenoids in bacteria holds great prospect.

In an ongoing search for structurally diverse sesquiterpenes from actinomycetes associated with animal feces, we systematically investigated the secondary metabolites of *Streptomyces fulvorobeus* (YIM 103582), which was isolated from *Elephas maximus* feces. The chemical analysis of fermentation broth of *S. fulvorobeus* led to obtain fifteen new compounds, (1*S*,2*R*,4*S*,5*S*,8*R*)-9-oxocaryolane-1,13-diol (**1**), (1*S*,2*R*,4*R*,5*S*,8*R*)-caryolane-1,14-diol (**2**), (1*S*,2*R*,4*R*,5*S*,8*R*,9*S*)-caryolane-1,9,14-triol (**3**), caryolane-1,6*α*,10*α*-triol (**4**), (2*S*,4*S*,7*S*,8*S*)-1(10)*E*,5*E*-germacradiene-2,8,11-triol (**13**), (2*S*,4*S*,7*R*)-1(10)*E*,5*E*-germacradiene-2,11-diol 2-methyl ether (**14**), (2*S*,4*R*,7*S*,8*S*)-1(10)*E*,5*E*-germacradiene-2,4,8,11-tetraol 2-acetate (**15**), (1*α*,3*α*,4*β*,5*α*,6*α*,7*β*,9*β*)-6,11-epoxyisodaucane-3,9-diol (**17**), 8*α*-hydroxyganodermanol L (**18**), (1*S*,2*S*,6*R*,7*S*,10*R*)-cadinane-2,10,15-triol (**22**), (1*R*,3*S*,6*R*,7*S*,9*S*,10*R*)-3,9-dihydroxyepicubenol (**23**), oplopanane-4,10*α*,11-triol (**25**), 4-*epi*-pallenane-4*α*,10,11-triol (**26**), 4-*epi*-pallenane-10,11-diol (**27**), (1*R*,3*S*,4*R*,7*R*,10*R*)-eudesm-5-ene-1,3,11-triol (**28**) as well as twenty-one known analogues. The

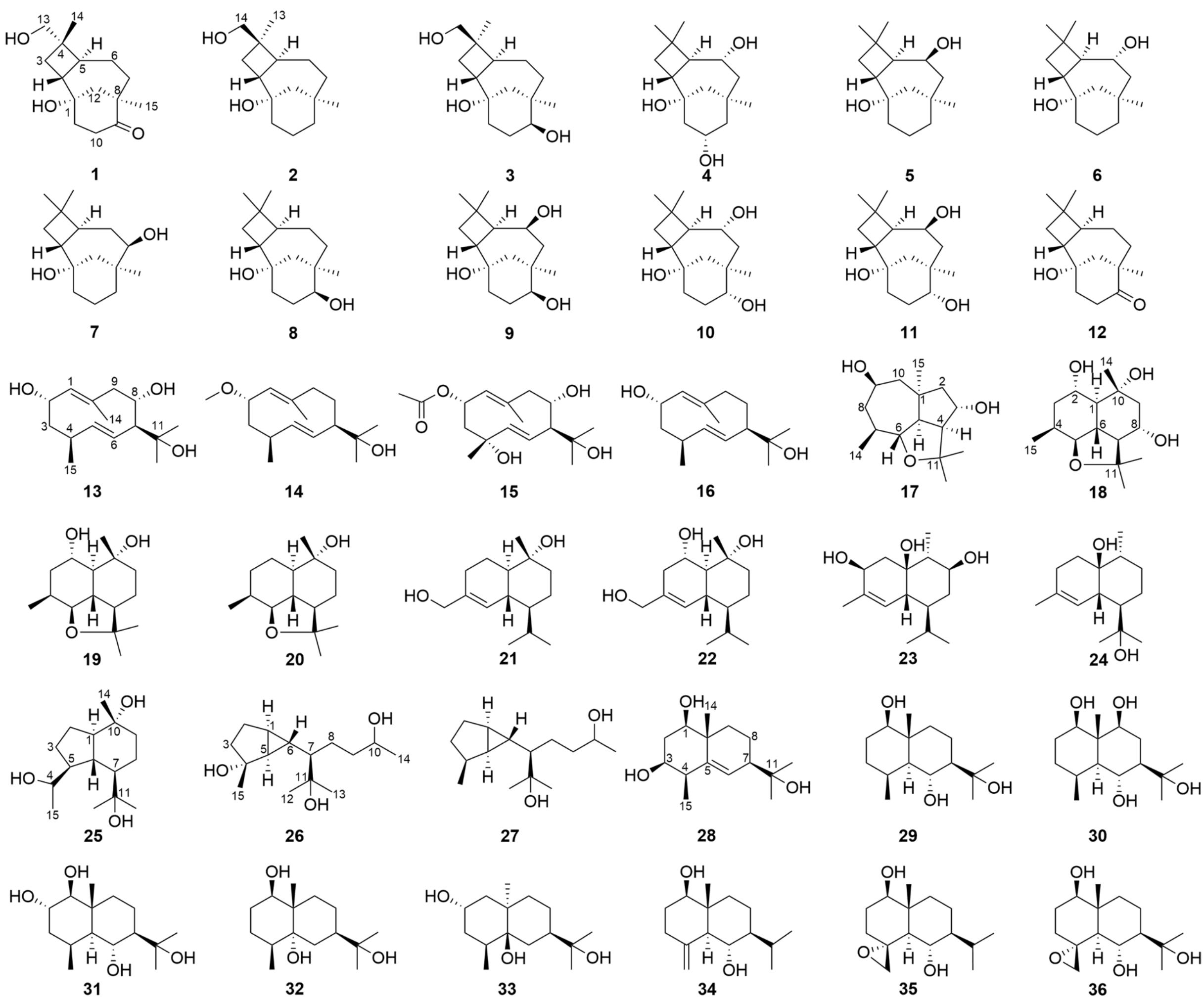

Fig. 1 Chemical structures of compounds **1–36** from *S. fulvorobeus*

types of structural skeleton include caryolane, germacrene, isodaucane, cadinane, epicubenol, oplopanane, pallenane, and eudesmane. The structures of the new compounds were elucidated based on detailed spectroscopic data analysis. In this study, we report the fermentation, isolation, structural elucidation, and evaluation of antimicrobial activities of the isolated compounds.

2 Results and discussion

The *S. fulvorobeus* was obtained from fresh feces of *E. maximus* collected in the Xishuangbanna National Nature Reserve. The fermentation broth of *S. fulvorobeus* was clarified with a centrifuge to collected 150 L of culture supernatant. The clarified supernatant was extracted with ethyl acetate and the extract was isolated by repeated column chromatography over silica gel, Sephadex LH-20, and ODS to afford thirty-six sequiterpenoids (Fig. 1).

2.1 Structural elucidation of isolated new compounds

Compound **1** was isolated as a colorless oil with the molecular formula $C_{15}H_{24}O_3$ based on HRESIMS and ^{13}C NMR data. The IR spectrum of **1** showed characteristic absorption bands for hydroxy groups (3382 cm^{-1}) and carbonyl (1699 cm^{-1}). The ^1H NMR (Table 1) of **1** displayed the presence of an oxygenated methylene (δ_H 3.14, 3.11), two singlet methyls (δ_H 1.01, 0.88), and other aliphatic residues at δ_H 0.98–2.82. The ^{13}C NMR data (Table 2) of **1** showed 15 carbons signals, including one carbonyl (δ_C 216.9), two oxygen bearing carbons (δ_C 71.0, 68.1), two quaternary carbons (δ_C 46.5, 38.4), six methylenes (δ_C 49.6, 38.6, 36.9, 34.7, 30.3, 26.4), two methines (δ_C 43.5, 39.9), and two methyls (δ_C 31.1, 17.7). Analysis of the 1D and 2D NMR data indicated that **1** was consistent with a caryolane-type sesquiterpenoid

Table 1 ^{1}H NMR (600 MHz, DMSO-d_6) spectroscopic data for compounds **1–4**

No	1	2	3	4
2	1.59, q (9.6)	2.22, brq (10.8)	2.27, brq (11.5)	1.86, brq (10.2)
3	1.78, t (10.2) 1.26, t (9.6)	1.61, m 1.40, m	1.59, m 1.35, m	1.50, t (10.0) 1.37, t (9.0)
5	1.82, m	1.85, dt (12.1, 7.6)	1.89, ddd (12.2, 9.4, 6.3)	1.61, dd (12.0, 8.4)
6	1.34, m 1.11, qd (12.6, 5.4)	1.48, m 1.38, m	1.49, m 1.37, m	3.51, m
7	1.87, m 0.98, td (12.7, 5.4)	1.50, m 1.00, m	1.58, m 0.87, m	1.51, m 1.15, dd (14.4, 7.8)
9		1.31, m 0.95, m	3.10, t (10.2)	1.57, dd (12.0, 4.2) 0.88, t (12.0)
10	2.82, ddd (16.6, 12.0, 4.8) 2.17, ddd (16.6, 9.6, 3.6)	1.63, m 1.53, m	1.63, m 1.58, m	3.68, m
11	1.84, m 1.70, m	1.45, m 1.16, td (12.0, 5.2)	1.43, m 1.30, m	1.74, brd (11.4) 1.05, m
12	1.89, brs 1.89, brs	1.57, brd (12.8) 0.91, brd (12.8)	1.46, m 0.89, m	1.83, brd (12.7) 0.92, d (12.7)
13	3.14, d (10.2) 3.11, d (10.2)	0.98, s	0.98, s	1.01, s
14	0.88, s	3.48, dd (10.6, 4.8) 3.40, dd (10.6, 5.4)	3.49, d (10.4) 3.42, d (10.4)	1.03, s
15	1.01, s	0.81, s	0.82, s	0.95, s
1-OH		3.94, s	3.97, brs	4.08, s
6-OH				4.08, s
9-OH			4.25, brs	
10-OH				4.37, s
14-OH		4.28, t (5.2)	4.33, brs	

Table 2 ^{13}C NMR (150 MHz, DMSO-d_6) spectroscopic data for compounds **1–4**, **13–15**

No	1	2	3	4	13	14	15
1	68.1, C	69.4, C	69.2, C	69.5, C	136.1, CH	131.4, CH	129.8, CH
2	43.5, CH	39.6, CH	37.5, CH	41.5, CH	63.8, CH	73.8, CH	69.3, CH
3	30.3, CH_2	30.6, CH_2	30.3, CH_2	35.5, CH_2	40.5, CH_2	40.0, CH_2	45.4, CH_2
4	38.4, C	39.7, C	39.9, C	34.1, C	32.3, CH	32.0, CH	70.5, C
5	39.9, CH	44.1, CH	43.4, CH	52.6, CH	139.7, CH	138.9, CH	142.1, CH
6	26.4, CH_2	21.5, CH_2	19.7, CH_2	70.2, CH	121.7, CH	125.6, CH	123.7, CH
7	38.6, CH_2	36.8, CH_2	30.1, CH_2	49.7, CH_2	61.8, CH	58.7, CH	60.9, CH
8	46.5, C	34.6, C	38.8, C	34.4, C	67.6, CH	21.9, CH_2	68.6, CH
9	216.9, C	37.6, CH_2	77.1, CH	48.6, CH_2	52.1, CH_2	41.4, CH_2	51.6, CH_2
10	34.7, CH_2	20.7, CH_2	30.0, CH_2	66.1, CH	132.9, C	138.2, C	137.7, C
11	36.9, CH_2	38.6, CH_2	38.3, CH_2	50.0, CH_2	73.4, C	70.8, C	73.4, C
12	49.6, CH_2	49.3, CH_2	48.4, CH_2	48.2, CH_2	30.8, CH_3	29.8, CH_3	30.8, CH_3
13	71.0, CH_2	26.6, CH_3	26.6, CH_3	31.8, CH_3	24.5, CH_3	26.0, CH_3	24.6, CH_3
14	17.7, CH_3	65.3, CH_2	65.3, CH_2	21.5, CH_3	18.4, CH_3	17.5, CH_3	18.4, CH_3
15	31.1, CH_3	33.6, CH_3	29.6, CH_3	36.9, CH_3	16.1, CH_3	16.0, CH_3	24.3, CH_3
2-OAc							169.9, C 21.5, CH_3
2-OCH_3						54.5, CH_3	

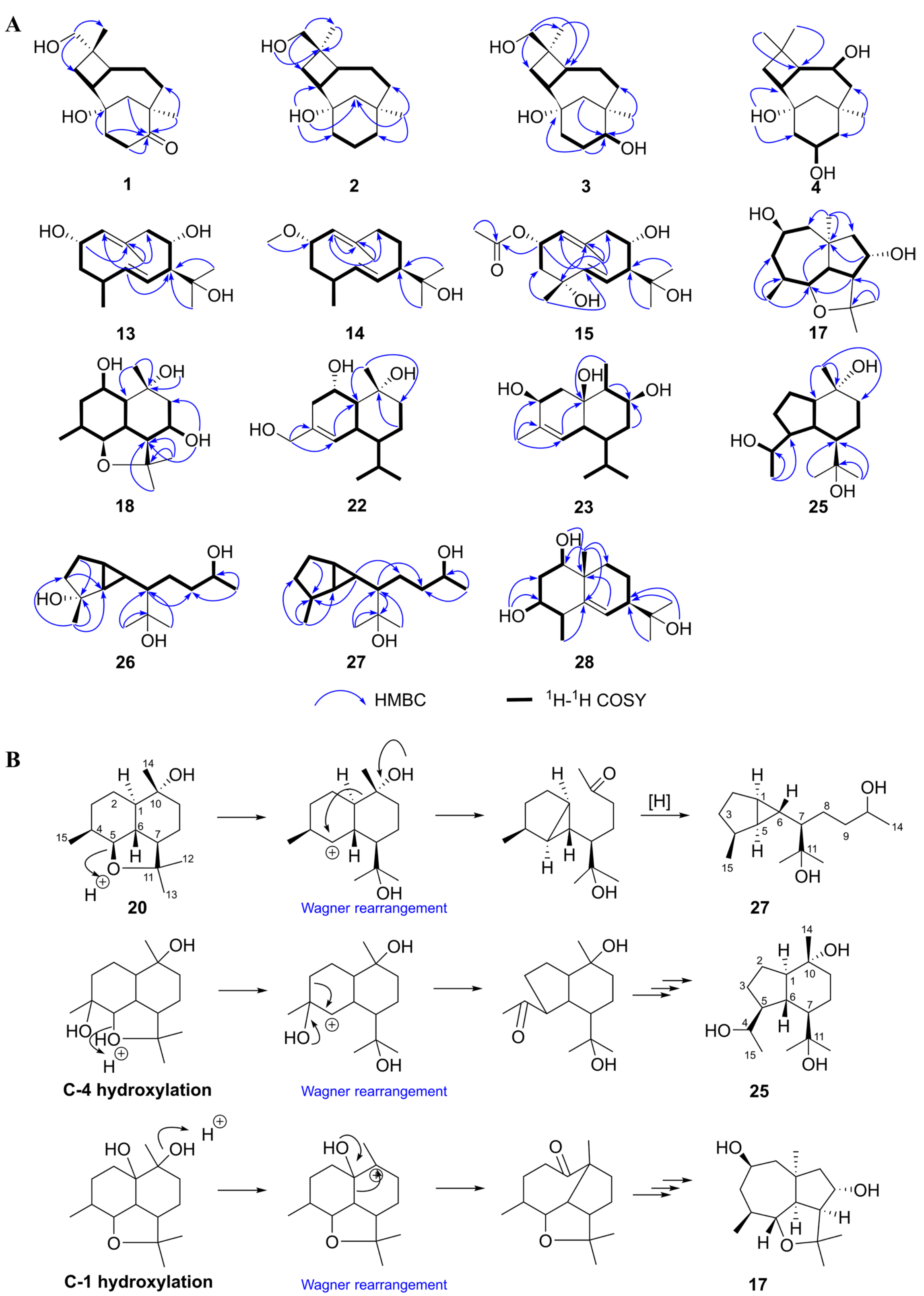

Fig. 2 Main HMBC and COSY correlations of compounds **1–4**, **13–15**, **17**, **18**, **22**, **23**, **25–28** (**A**). proposed biosynthetic pathway of compounds **17**, **25**, **27** (**B**)

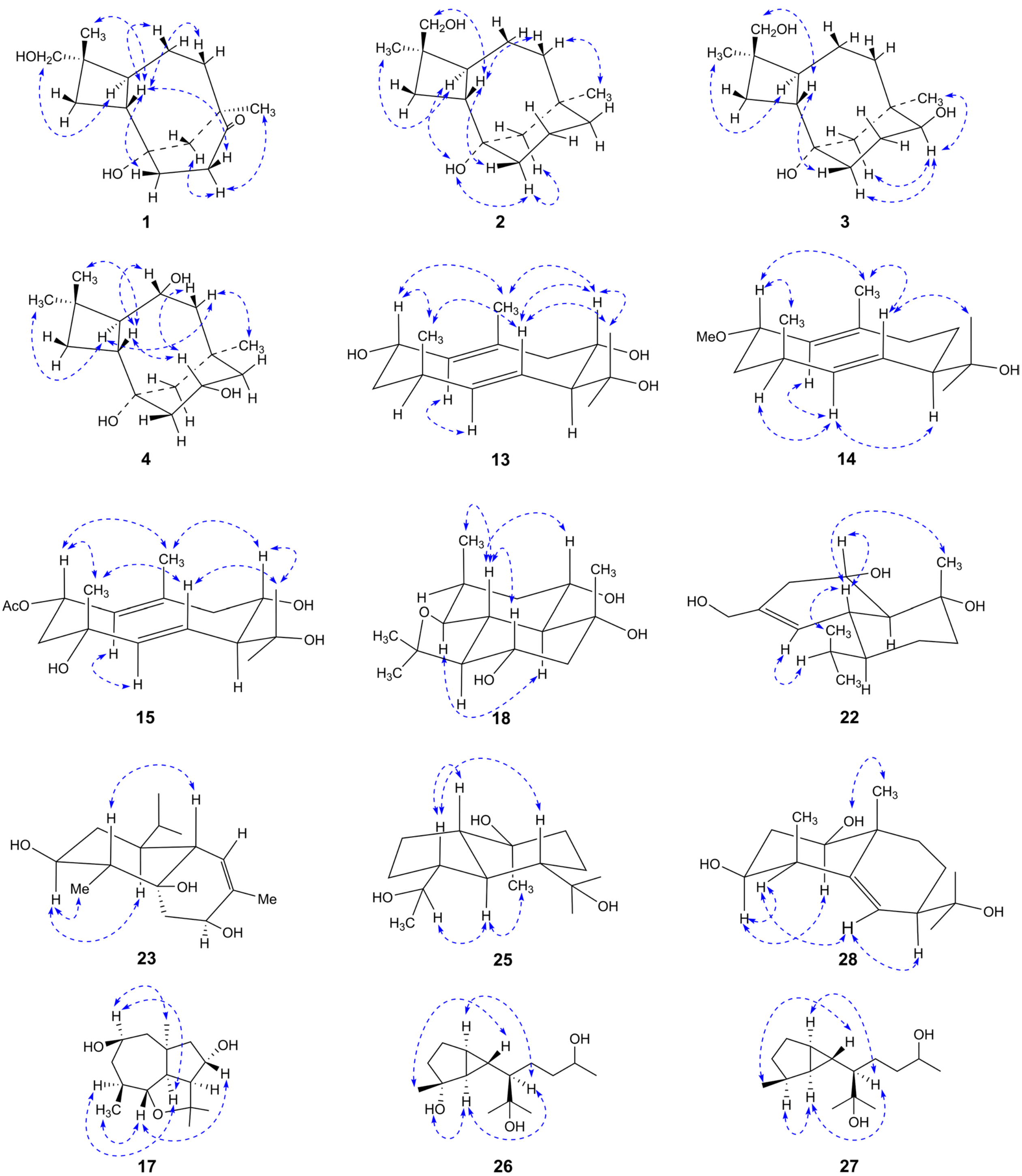

Fig. 3 Main NOE correlations of compounds **1–4**, **13–15**, **17**, **18**, **22**, **23**, **25–28**

and exhibited similarity to the reported bacaryolane A [19], except for the presence of an additional hydroxymethyl (δ_C 71.0, δ_H 3.14, 3.11) and the absence of a methyl. The HMBC correlations from H-13 (δ_H 3.14, 3.11) to C-3 (δ_C 30.3) and C-14 (δ_C 17.7), from H-3β (δ_H 1.78) to C-13 (δ_C 71.0), and from H-14 (δ_H 0.88) to C-13 (δ_C 71.0) established the hydroxymethyl was located at C-4. Moreover, the HMBC correlations from H-10 (δ_H 2.82,

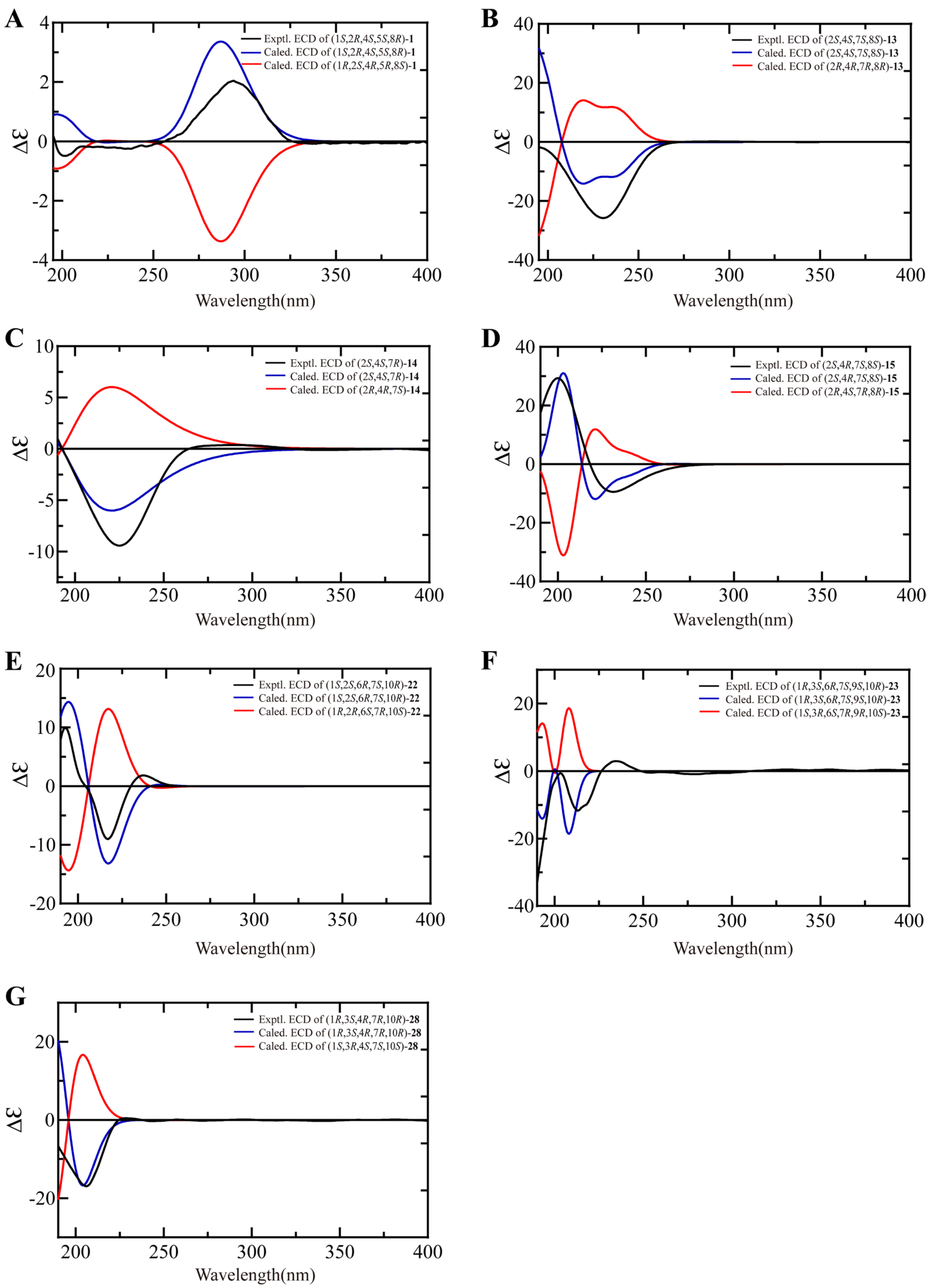

Fig. 4 Experimental ECD spectra and calculated ECD spectra of compounds **1** (**A**), **13–15** (**B–D**), **22** (**E**), **23** (**F**), **28** (**G**)

2.17), H-11 (δ_H 1.84, 1.70), H-12 (δ_H 1.89), and H_3-15 (δ_H 1.01) to C-9 (δ_C 216.9) confirmed that the carbonyl was located at C-9 (Fig. 2A). Caryolanes derived from plants and bacteria possessed varied stereochemical structures as they were biosynthesized by different cyclization from the humulyl cation [19]. The carbon skeleton of caryolanes in the current study was defined the same as those from bacteria such as bacaryolanes A-C [19]. The NOESY correlations found between H-13 (δ_H 3.14, 3.11) and H-5 (δ_H 1.82), between H_3-14 (δ_H 0.88) and H-2 (δ_H 1.59) established that H-2 and H_3-14 were *β*-orientated, whereas H-5 and H_2-13 were *α*-orientated. In addition, NOE correlations between H_3-15 (δ_H 1.01) and H-10*α* (δ_H 2.82), between H-10*β* (δ_H 2.17) and H-2 (δ_H 1.59) further confirmed the structure (Fig. 3). The absolute configuration 1*S*,2*R*,4*S*,5*S*,8*R* were deduced from comparison of experimental and calculated ECD spectra of **1** (Fig. 4A). According to the literature, the proton signals of the oxymethylene protons in the (*S*)- and (*R*)-*α*-methoxy-*α*-trifluoromethylphenylacetyl (MTPA) esters of primary alcohol showed a unique split pattern [24]. **1** was treated with (*R*)-MTPA-Cl and (*S*)-MTPA-Cl to afford the (*S*)- or (*R*)-MTPA ester derivatives **1a** and **1b**, respectively. The signals of oxymethylene protons at C-13 for the (*S*)-MTPA ester **1a** appeared at δ_{low} 4.26 and δ_{high} 4.24 ($\Delta\delta$ 0.02), while those for the (*R*)-MTPA ester **1b** were observed as two separated doublet signals at δ_{low} 4.30 and δ_{high} 4.22 ($\Delta\delta$ 0.08). The (*R*)-MTPA esters of primary alcohol analogue possessing 4*S*-configuration had relatively larger $\Delta\delta$ ($\delta_{low}-\delta_{high}$) values. Therefore, the structure of **1** was elucidated as (1*S*,2*R*,4*S*,5*S*,8*R*)-9-oxocaryolane-1,13-diol.

Compound **2** had the molecular formula $C_{15}H_{26}O_2$ by its HRESIMS and ^{13}C NMR data. Its ^1H and ^{13}C NMR data revealed that **2** was a caryolane type sesquiterpenoid and related to the known compound caryolan-1-ol [25]. The distinct difference was that a methyl of caryolan-1-ol was replaced by a hydroxymethyl (δ_C 65.3, δ_H 3.48, 3.40) in **2**. The HMBC correlations between H-14 (δ_H 3.48, 3.40) and C-3 (δ_C 30.6) and C-13 (δ_C 26.6), between H-3 (δ_H 1.61, 1.40), H-13 (δ_H 0.98) and C-14 (δ_C 65.3) determined the hydroxymethyl at C-4 (Fig. 2A). NOE correlations between H-5 (δ_H 1.85) and 1-OH (δ_H 3.94), H_3-13 (δ_H 0.98), between H-2 (δ_H 2.22) and H-14

Table 3 ^1H NMR (600 MHz, DMSO-d_6) spectroscopic data for compounds **13–15**, **17**, **18**

No	13	14	15	17	18
1	4.90, d (9.6)	4.80, d (10.2)	4.82, d (10.2)		1.22, dd (12.5, 9.7)
2	4.19, td (10.2, 4.2)	3.90, td (10.2, 3.6)	5.21, dd (11.4, 4.2)	1.82, m 1.53, dd (13.8, 3.6)	3.67, brt (9.6)
3	1.67, dt (13.2, 4.2) 1.37, ddd (12.6, 10.8, 3.6)	1.76, dt (13.2, 4.2) 1.52, ddd (13.8, 10.8, 3.6)	1.76, dd (12.0, 3.6) 1.48, t (12.0)	4.17, quint (5.6)	1.69, ddd (13.8, 4.2, 3.0) 1.42, m
4	2.41, m	2.41, m		2.30, dd (8.4, 4.8)	2.05, m
5	5.41, dd (15.6, 3.6)	5.35, dd (15.6, 3.0)	5.20, d (15.6)	1.94, t (9.5)	3.46, dd (10.2, 4.8)
6	4.65, ddd (15.6, 10.2, 2.4)	4.84, ddd (15.6, 9.6, 1.8)	4.72, dd (15.6, 10.2)	3.13, t (9.9)	1.16, m
7	2.28, m	2.10, brq (10.8)	2.25, t (10.2)	1.42, m	1.38, m
8	3.80, td (9.6, 3.6)	1.71, m 1.24, brq (11.4)	3.87, td (10.2, 4.2)	1.82, m 1.04, q (12.0)	3.38, m
9	2.27, m 2.25, m	2.27, dd (12.6, 4.2) 2.16, td (12.6, 1.8)	2.32, dd (12.3, 9.7) 2.29, dd (12.3, 4.0)	3.51, td (10.2, 1.8)	1.77, dd (12.0, 3.6) 1.40, m
10				1.62, brd (13.6) 1.48, dd (13.6, 10.2)	
12	0.93, s	0.99, s	0.98, s	1.17, s	1.26, s
13	1.14, s	0.94, s	1.14, s	1.17, s	1.07, s
14	1.53, s	1.57, s	1.61, s	0.87, d (6.0)	1.17, s
15	0.97, d (6.6)	1.02, d (6.6)	1.15, s	1.16, s	0.84, d (7.2)
2-OH					4.34, d (3.0)
2-OAc			1.93, s		
2-OCH_3		3.06, s			
8-OH					4.56, d (5.4)
10-OH					4.33, s
11-OH		4.04, s			

(δ_H 3.48, 3.40), H-7β (δ_H 1.50), between H-7α (δ_H 1.00) and H_3-15 (δ_H 0.81) indicated that H-2, H-14 were β-orientation whereas 1-OH, H-5, H_3-13, H_3-15 were α-orientation (Fig. 3). The absolute configuration of C-4 was determined by Mosher's method. Treatment of **2** with (*R*)-MTPA-Cl or (*S*)-MTPA-Cl obtained the *S* or *R* Mosher's esters **2a** and **2b**. The signals of oxymethylene protons at C-14 for the (*S*)-MTPA ester **2a** showed two separated doublet signals at δ_{low} 4.69 and δ_{high} 4.55 ($\Delta\delta$ 0.14), while those for the (*R*)-MTPA ester **2b** were presented at δ_H 4.63 as a broad singlet peak. These findings suggested the *R*-configuration of C-4 in **2** by comparing the $\Delta\delta$ values of oxymethylene protons with those of 4*S*-configuration analogue **1**. Thus, **2** was deduced to be (1*S*,2*R*,4*R*,5*S*,8*R*)-caryolane-1,14-diol as the same biosynthesis pathway from bacteria.

Compound **3** afforded a molecular formula of $C_{15}H_{26}O_3$ on the basis of HRESIMS and ^{13}C NMR data. Analysis of its ^{1}H and ^{13}C NMR data (Tables 1, 2) indicated that **3** has a close structural relationship to **2**. The only difference was that one methylene was absent and one oxygenated methine was present (δ_C 77.1, δ_H 3.10) in **3**. The HMBC correlations from H-10 (δ_H 1.63, 1.58), H-12 (δ_H 1.46, 0.89), H_3-15 (δ_H 0.82) to C-9 (δ_C 77.1) as well as ^{1}H–^{1}H COSY correlations between H-9 (δ_H 3.10) and H-10 (δ_H 1.63, 1.58) confirmed a hydroxy at C-9 (Fig. 2A). The NOE cross peaks observed between H_3-13 (δ_H 0.98) and H-5 (δ_H 1.89), between H_3-15 (δ_H 0.82) and H-9 (δ_H 3.10), between H-9 (δ_H 3.10) and H-11α (δ_H 1.30), and between H-2 (δ_H 2.27) and H-14 (δ_H 3.49, 3.42) and H-11β (δ_H 1.43) indicated that H-2, H-14, and 9-OH were β-oriented, while H-5, H-9, H_3-13, and H_3-15 were α-oriented (Fig. 3). The (*S*)-MTPA ester (3a) or (*R*)-MTPA ester (3b) were obtained by the same derivative process as those of **1** and **2**. Both 9-OH and 14-OH in compound **3** were esterified by MTPA-Cl according to NMR data. Unfortunately, it was impossible to assign the absolute configuration of C-4 as the $\Delta\delta$ values of two separated peaks of H_2-14 for 3a and 3b were very approximate ($\Delta\delta = 0.12$ for **3a** and $\Delta\delta = 0.10$ for **3b**) being influenced by two MTPA groups. As **3** presented almost identical ^{13}C NMR data of C-4, C-13, and C-14 with those of compound **2**, the *R*-configuration of C-4 could be determined. The configuration of C-9 could be deduced by comparing the chemical shift of H_3-15 in (*S*)- and (*R*)-MTPA esters. The signal of H_3-15 for (*S*)-MTPA ester 3a was observed at lower field (δ_H 0.99) compared to the signal for (*R*)-MTPA ester **3b** (δ_H 0.88), which exhibited the absolute configuration of C-9 to be *S*. Thus, the structure of **3** was confirmed as (1*S*,2*R*,4*R*,5*S*,8*R*,9*S*)-caryolane-1,9,14-triol.

The molecular formula of **4** was deduced as $C_{15}H_{26}O_3$ according to its HRESIMS and ^{13}C NMR data. The ^{1}H NMR and ^{13}C NMR data (Tables 1, 2) indicated that **4** was similar to bacaryolane C (**6**) [19], also isolated in the current study. The obvious alteration was that a methylene in **6** was replaced by an oxygenated methine (δ_C 66.1, δ_H 3.68) in **4**. The HMBC correlations from H-9 (δ_H 1.57, 0.88), H-11 (δ_H 1.74, 1.05) to C-10 (δ_C 66.1) confirmed that a hydroxy was located at C-10. The COSY correlations from H-10 (δ_H 3.68) to H-9 (δ_H 1.57, 0.88), H-11 (δ_H 1.74, 1.05), and 10-OH (δ_H 4.37) further supported the above inference (Fig. 2A). The NOESY cross peaks from H-2 (δ_H 1.86) to H-6 (δ_H 3.51) and H-10 (δ_H 3.68), from H-10 (δ_H 3.68) to H-7β (δ_H 1.51) indicated that H-2, H-6, and H-10 were on the same side. Correspondingly, the NOESY correlations from H_3-15 (δ_H 0.95) to H-7α (δ_H 1.15), from H-7α (δ_H 1.15) to H-5 (δ_H 1.61) suggested that H-5, H_3-15 were on the opposite side (Fig. 3). Consequently, **4** was deduced to be caryolane-1,6α,10α-triol.

Compound **13** was isolated as a colorless oil with a molecular formula $C_{15}H_{26}O_3$ by HRESIMS and ^{13}C NMR data. Its IR spectrum revealed the presence of hydroxy groups (3315 cm^{-1}) and double bonds (1668 cm^{-1}). The ^{1}H NMR data (Table 3) showed three olefinic hydrogens (δ_H 5.41, 4.90, 4.65), two oxygenated methines (δ_H 4.19, 3.80), three singlet methyls (δ_H 1.53, 1.14, 0.93), one doublet methyl (δ_H 0.97), and other aliphatic hydrogens (δ_H 1.37–2.41). The ^{13}C NMR data (Table 2) of **13** displayed 15 carbon signals, including four olefinic carbons (δ_C 139.7, 136.1, 132.9, 121.7), three oxygen-bearing carbons (δ_C 73.4, 67.6, 63.8), two methines (δ_C 61.8, 32.3), two methylenes (δ_C 52.1, 40.5), and four methyls (δ_C 30.8, 24.5, 18.4, 16.1), as determined in an HSQC experiment. The ^{1}H and ^{13}C NMR data of **13** were very similar to those of 1(10)*E*,5*E*-germacradiene-2α,11-diol (**16**) [26], a germacrane-type sesquiterpenoid. The major differences were the disappearance of a methylene in **16** and the existence of an oxygen-bearing methine (δ_C 67.6, δ_H 3.80) in **13**. The ^{1}H–^{1}H COSY correlations from H-8 (δ_H 3.80) to H-7 (δ_H 2.28) and H-9 (δ_H 2.27, 2.25) as well as the HMBC correlations between H-7 (δ_H 2.28), H-9 (δ_H 2.27, 2.25) and C-8 (δ_C 67.6) indicated that a hydroxy was connected with C-8 (Fig. 2A). Thus, the planar structure of compound **13** was established. The NOE interactions observed between H-2 (δ_H 4.19) and H_3-15 (δ_H 0.97), between H-6 (δ_H 4.65) and H-8 (δ_H 3.80), H_3-15 (δ_H 0.97), between H_3-13 (δ_H 1.14) and H-6 (δ_H 4.65), H-8 (δ_H 3.80) revealed that H-2, H-8, and H_3-15 were on the same side, while 2-OH, 8-OH, H-4, and H-7 were located on the opposite side (Fig. 3). Furthermore, the coupling constants of H-2 (δ_H 4.19, td, $J = 10.2$, 4.2 Hz) suggested that the 2-OH presented in the equatorial position. In addition, NOE interactions observed from H_3-14 (δ_H 1.53) to H-2 (δ_H 4.19) and H-8 (δ_H 3.80), from H-1 (δ_H 4.90) to H-5 (δ_H 5.41) as well as the large coupling constant of H-5/H-6 elucidated the *E* configurations of C-1/C-10 and

Table 4 ^{13}C NMR (150 MHz, DMSO-d_6) spectroscopic data for compounds **17**, **18**, **22**, **23**, **25–28**

No	17	18	22	23	25	26	27	28
1	38.9, C	52.9, CH	53.8, CH	74.6, C	58.9, CH	23.8, CH	23.8, CH	76.5, CH
2	51.9, CH_2	66.7, CH	70.1, CH	34.3, CH_2	25.7, CH_2	26.2, CH_2	28.0, CH_2	35.6, CH_2
3	73.0, CH	39.8, CH_2	36.9, CH_2	68.0, CH	24.2, CH_2	37.2, CH_2	30.2, CH_2	68.7, CH
4	64.2, CH	31.0, CH	136.9, C	136.4, C	67.2, CH	78.8, C	35.0, CH	45.5, CH
5	61.6, CH	80.8, CH	120.7, CH	124.2, CH	48.1, CH	36.3, CH	30.1, CH	145.9, C
6	82.3, CH	40.0, CH	40.5, CH	47.4, CH	44.3, CH	23.1, CH	18.9, CH	126.6, CH
7	38.2, CH	59.1, CH	46.5, CH	45.7, CH	55.5, CH	52.0, CH	52.1, CH	48.2, CH
8	47.7, CH_2	67.0, CH	21.8, CH_2	34.3, CH_2	28.4, CH_2	27.6, CH_2	27.7, CH_2	21.1, CH_2
9	66.7, CH	52.8, CH_2	41.4, CH_2	71.3, CH	42.8, CH_2	39.4, CH_2	39.4, CH_2	38.3, CH_2
10	51.7, CH_2	74.1, C	73.0, C	51.3, CH	71.2, C	67.1, CH	67.1, CH	39.3, C
11	80.0, C	83.0, C	26.5, CH	26.6, CH	72.4, C	72.9, C	73.0, C	71.5, C
12	24.8, CH_3	24.4, CH_3	15.4, CH_3	15.5, CH_3	24.5, CH_3	26.5, CH_3	26.3, CH_3	28.2, CH_3
13	32.8, CH_3	31.1, CH_3	21.8, CH_3	22.0, CH_3	31.9, CH_3	30.6, CH_3	30.7, CH_3	25.6, CH_3
14	20.3, CH_3	23.4, CH_3	21.7, CH_3	11.5, CH_3	20.6, CH_3	24.2, CH_3	24.3, CH_3	21.1, CH_3
15	31.3, CH_3	11.9, CH_3	64.9, CH_2	20.3, CH_3	23.3, CH_3	26.4, CH_3	18.9, CH_3	16.7, CH_3

C-5/C-6 double bonds. The experimental ECD spectrum of **13** had a consistent trend with its corresponding calculated ECD curve which determined the 2*S*,4*S*,7*S*,8*S*-configurations (Fig. 4B). Consequently, **13** was established as (2*S*,4*S*,7*S*,8*S*)-1(10)*E*,5*E*-germacradiene-2,8,11-triol.

The ^{1}H and ^{13}C NMR data (Tables 2, 3) as well as a molecular formula of $C_{16}H_{28}O_2$ exhibited that **14** bore a close resemblance to the known compound **16** [26], except for the presence of an additional methoxy (δ_C 54.5, δ_H 3.06). The HMBC correlation between methoxy (δ_H 3.06) and C-2 (δ_C 73.8) determined that the methoxy was located at C-2 (Fig. 2A). In NOESY spectrum, the key cross peaks from H-2 (δ_H 3.90) to H_3-15 (δ_H 1.02), from H-5 (δ_H 5.35) to H-4 (δ_H 2.41) and H-7 (δ_H 2.10) indicated that H-2 and H_3-15 were β-orientation, while H-4 and H-7 were α-orientation (Fig. 3). Moreover, the double bonds at C-5/C-6, C-1/C-10 were elucidated as *E* geometry based on the NOE correlations from H_3-14 (δ_H 1.57) to H-2 (δ_H 3.90) and H-6 (δ_H 4.84), from H-1 (δ_H 4.80) to H-5 (δ_H 5.35) as well as the large coupling constant of H-5/H-6 (J=15.6 Hz). The absolute configurations of C-2, C-4, and C-7 were elucidated as 2*S*,4*S*,7*R* based on comparing the experimental and calculated ECD spectra (Fig. 4C). Therefore, the structure of **14** was confirmed as (2*S*,4*S*,7*R*)-1(10)*E*,5*E*-germacradiene-2,11-diol 2-methyl ether.

Compound **15** was assigned a molecular formula of $C_{17}H_{28}O_5$ based on its HRESIMS and ^{13}C NMR data. The characteristic ^{1}H and ^{13}C NMR data (Tables 2, 3) of **15** suggested that it was a germacrane-type sesquiterpenoid and had a close structural relationship to **13**, except for the different oxygenated position and an additional acetyl (δ_C 169.9, 21.5). HMBC correlations from H-3 (δ_H 1.76, 1.48), H-6 (δ_H 4.72) and H_3-15 (δ_H 1.15) to C-4 (δ_C 70.5) confirmed that the extra hydroxy was located at C-4. HMBC correlations from H-2 (δ_H 5.21) to C-16 (δ_C 169.9) as well as ^{1}H–^{1}H COSY correlations from H-2 (δ_H 5.21) to H-1 (δ_H 4.82) and H-3 (δ_H 1.76, 1.48) indicated that the acetyl was located at C-2. (Fig. 2A). **15** presented the same relative configuration as those of **13** and **14** on the basis of NOE correlations between H-2 (δ_H 5.21) and H_3-15 (δ_H 1.15), H_3-14 (δ_H 1.61), between H_3-14 (δ_H 1.61) and H-8 (δ_H 3.87), between H_3-13 (δ_H 1.14) and H-6 (δ_H 4.72), H-8 (δ_H 3.87) (Fig. 3). Besides, the geometry at C-5/C-6 double bonds was assigned as *E* according to the large coupling constants of H-5/H-6 (J=15.6 Hz). The (+) Cotton effect at 200 nm (+29.25) and (−) Cotton effect at 231 nm (−9.42) of **15** detected by CD spectrum was consistent with those of the calculated ECD curve of 2*S*,4*R*,7*S*,8*S*-**15** (Fig. 4D). Thus, **15** was identified as (2*S*,4*R*,7*S*,8*S*)-1(10)*E*,5*E*-germacradiene-2,4,8,11-tetraol 2-acetate.

The HRESIMS and ^{13}C NMR data determined the molecular formula of **17** as $C_{15}H_{26}O_3$. The NMR data (Tables 3, 4) suggested **17** was a 6,11-epoxyisodaucane type sesquiterpenoid and related to the known compound 6,11-epoxyisodaucane [27]. The difference was that two oxygenated methines replaced two methylenes in **17**. ^{1}H–^{1}H COSY correlations from H-3 (δ_H 4.17) to H-4 (δ_H 2.30) and H-2 (δ_H 1.82, 1.53), from H-9 (δ_H 3.51) to H-10 (δ_H 1.62, 1.48) and H-8 (δ_H 1.82, 1.04) determined the two hydroxys at C-3 and C-9, respectively. The HMBC correlations between H_3-15 (δ_H 1.16) and C-1 (δ_C 38.9), C-2 (δ_C 51.9), C-5 (δ_C 61.6), and C-10 (δ_C 51.7), between H-6 (δ_H 3.13) and C-1 (δ_C 38.9), C-8 (δ_C 47.7), between H-5 (δ_H 1.94) and C-2 (δ_C 51.9), C-3 (δ_C

Table 5 ^{1}H NMR (600 MHz, DMSO-d_6) spectroscopic data for compounds **22**, **23**, **25–28**

No	22	23	25	26	27	28
1	1.30, t (10.6)		1.26, m	1.04, m	0.97, m	3.03, dt (11.6, 4.8)
2	3.82, td (10.2, 6.0)	1.80, dd (12.8, 6.8) 1.19, m	1.53, m 1.00, m	1.87, m 1.56, dd (12.0, 7.9)	1.65, m 1.65, m	1.65, brq (12.0) 1.60, m
3	2.20, dd (16.2, 4.8) 1.89, m	3.96, brt (8.0)	1.66, ddd (11.5, 7.8, 3.0) 1.22, m	1.34, dd (13.4, 8.4) 1.11, m	1.54, m 0.70, dq (12.8, 10.0)	3.52, m
4			4.23, m		2.15, m	2.39, quint (7.0)
5	5.61, s	5.33, d (5.6)	2.00, brt (9.0)	1.13, dd (6.0, 3.6)	1.12, dt (6.3, 3.5)	
6	1.73, brt (10.6)	1.56, dd (11.2, 4.8)	1.37, td (10.9, 8.0)	0.13, dt (10.3, 3.4)	0.27, dt (10.3, 3.3)	5.53, m
7	1.02, m	1.16, m	1.18, ddd (13.3, 10.5, 3.0)	0.57, ddd (10.0, 8.0, 3.5)	0.56, ddd (10.6, 7.8, 3.5)	2.02, ddd (11.0, 6.2, 2.0)
8	1.51, m 1.04, m	1.67, dt (11.6, 4.3) 0.91, brd (11.6)	1.61, dt (13.3, 3.5) 0.95, m	1.62, m 1.26, m	1.65, m 1.27, m	1.56, m 1.19, m
9	1.61, dt (12.6, 3.0) 1.38, td (12.6, 3.6)	3.00, td (10.8, 4.4)	1.57, dt (12.6, 3.4) 1.28, m	1.60, m 1.25, m	1.61, m 1.25, m	1.80, dt (12.4, 3.2) 1.06, m
10		1.23, m		3.50, m	3.51, m	
11	2.10, m	1.95, m				
12	0.73, d (7.2)	0.78, d (7.2)	1.02, s	1.05, s	1.06, s	1.04, s
13	0.88, d (6.6)	0.86, d (7.2)	1.09, s	1.16, s	1.16, s	0.97, s
14	1.18, s	0.96, d (6.4)	0.98, s	1.04, d (6.1)	1.03, d (6.1)	0.95, s
15	3.77, brd (10.8) 3.75, brd (10.8)	1.64, s	0.94, d (6.3)	1.22, s	0.99, d (6.6)	0.96, d (6.4)
1-OH						4.45, d (4.8)
3-OH						4.50, d (4.0)
4-OH			4.04, d (5.6)	4.24, s		
10-OH			4.03, s	4.26, d (4.4)	4.27, brs	
11-OH			4.08, brs	3.95, s	3.93, brs	4.15, s

73.0), C-10 (δ_C 51.7), and C-15 (δ_C 31.3), between H-12 (δ_H 1.17) and C-4 (δ_C 64.2), C-11 (δ_C 80.0) confirmed the planar structure (Fig. 2A). The absolute configuration of 6,11-epoxyisodaucane was determined by total synthesis method [27]. The similar coupling constants of H-5 (δ_H 1.94, t, $J=9.5$ Hz), H-6 (δ_H 3.13, t, $J=9.9$ Hz) indicated that **17** possessed the same 4α-H, 5α-H, 6β-H, 7β-methyl configuratinos as those of synthesized 6,11-epoxyisodaucane. The NOE interactions from H-5 (δ_H 1.94) to H-9 (δ_H 3.51), H-7 (δ_H 1.42), from H_3-14 (δ_H 0.87) to H-6 (δ_H 3.13), from H-6 (δ_H 3.13) to H-3 (δ_H 4.17), from H_3-15 (δ_H 1.16) to H-9 (δ_H 3.51) determined the configurations as in Fig. 3.

Analysis of ^{1}H NMR, ^{13}C NMR (Tables 3, 4), and HRESIMS data of **18** indicated it was a sesquiterpenoid and was related to the reported ganodermanol L (**19**) [28]. The only difference was one more oxygenated methine (δ_C 67.0, δ_H 3.38) in **18** replaced a methylene in **19**. The HMBC correlations between 8-OH (δ_H 4.56) and C-7 (δ_C 59.1), C-8 (δ_C 67.0), and C-9 (δ_C 52.8) determined the C-8 position of extra hydroxy. Moreover, COSY correlations from H-8 (δ_H 3.38) to H-7 (δ_H 1.38), H-9 (δ_H 1.77, 1.40), and 8-OH (δ_H 4.56) further supported the conclusion (Fig. 2A). NOE cross peaks observed between H-6 (δ_H 1.16) and H-2 (δ_H 3.67), H-8 (δ_H 3.38), H_3-15 (δ_H 0.84), between H-5 (δ_H 3.46) and H-1 (δ_H 1.22) demonstrated that H-2, H-6, H-8, and H_3-15 were located on the same side, whereas H-1, H-5, and H-7 were located on the opposite side (Fig. 3). There were potential inaccuracies of NOE correlations due to the overlapped signals of H-6 (δ_H 1.16) and H_3-14 (δ_H 1.17). The configuration of C-10 was then confirmed through comparing the ^{13}C NMR data of C-1, C-2, C-10, and C-14 with those of ganodermanol L (**19**) [28], which was elucidated the structure by X-ray crystallographic analyses. In addition, the peak shapes and coupling constants of H-1 (δ_H 1.22, dd, $J=12.5$, 9.7 Hz), H-2 (δ_H 3.67, brt $J=9.6$ Hz), and H-5 (δ_H 3.46, dd, $J=10.2$, 4.8 Hz) further confirmed the relative configuration.

The ^{1}H and ^{13}C NMR data (Tables 4, 5) as well as molecular formula, $C_{15}H_{26}O_3$, of **22** showed it was a cadinene-type sesquiterpenoid and related to 15-hydroxy-α-cadinol

(**21**) [29], except an additional oxygenated methine (δ_C 70.1, δ_H 3.82) in **22** instead of a methylene in **21**. ^1H–^1H COSY correlations from H-2 (δ_H 3.82) to H-3 (δ_H 2.20, 1.89) and H-1 (δ_H 1.30) as well as HMBC correlations from H-1 (δ_H 1.30), H-3 (δ_H 2.20, 1.89) to C-2 (δ_C 70.1) revealed that a hydroxy was located at C-2 (Fig. 2A). The large coupling constants of H-1 (δ_H 1.30, brt, $J=10.6$ Hz), H-6 (δ_H 1.73, brt, $J=10.6$ Hz) indicated a *trans* fusion of the bicyclic system. NOE correlations from H-6 (δ_H 1.73) to H-2 (δ_H 3.82), H_3-14 (δ_H 1.18), and H_3-12 (δ_H 0.73) indicated that the H-2, H-6, and H_3-14 were *β*-orientated, whereas H-1, H-7, 2-OH, and 10-OH were *α*-orientated (Fig. 3). Comparison of the experimental and calculated ECD spectra of **22** revealed the absolute configuration as 1*S*,2*S*,6*R*,7*S*,10*R* (Fig. 4E). Thus, compound **22** was elucidated as (1*S*,2*S*,6*R*,7*S*,10*R*)-cadinane-2,10,15-triol.

The molecular formula of **23** was determined to be $C_{15}H_{26}O_3$ according to HRESIMS and ^{13}C NMR data. Analysis of its ^1H and ^{13}C NMR data (Tables 4, 5) indicated that **23** possessed a resemble structural relationship to 3*β*-hydroxyepicubenol [13], except for one oxygenated methine (δ_C 71.3, δ_H 3.00) instead of a methylene in **23**. ^1H–^1H COSY correlations from H-9 (δ_H 3.00) to H-8 (δ_H 1.67, 0.91) and H-10 (δ_H 1.23) supported that an additional hydroxy was located at C-9. This conclusion was confirmed by HMBC correlations between H-8 (δ_H 1.67, 0.91), H-10 (δ_H 1.23) and C-9 (δ_C 71.3) (Fig. 2A). The relative configuration of **23** was established from detailed analysis of NOE correlations. NOE interactions from H-9 (δ_H 3.00) to H-7 (δ_H 1.16) and H_3-14 (δ_H 0.96), from H-6 (δ_H 1.56) to H-10 (δ_H 1.23) revealed that H-7, H-9, and H_3-14 were *α*-orientation, while H-6 and H-10 were *β*-orientation (Fig. 3). Although there was no obvious NOE correlation to demonstrate the configuration of 1-OH and 3-OH, comparing the ^{13}C NMR data of C-1 (δ_C 74.6), C-2 (δ_C 34.3), C-3 (δ_C 68.0), C-4 (δ_C 136.4), C-5 (δ_C 124.2), and C-6 (δ_C 47.4) of **23** with those of the analogues indicated that **23** possessed the same configurations of C-1 and C-3 as 3*β*-hydroxyepicubenol [13] and muurol-4-ene-1*β*,3*β*,10*β*-triol [30]. The absolute configurations of the chiral carbons were determined to be 1*R*,3*S*,6*R*,7*S*,9*S*,10*R* according to the experimental ECD spectrum of **23** closely matched the calculated ECD curve (Fig. 4F).

Compound **25** had a molecular formula of $C_{15}H_{28}O_3$ from its HRESIMS and ^{13}C NMR data. The characteristic ^1H and ^{13}C NMR data (Tables 4, 5) of **25** demonstrated an oplopanane sequiterpenoid and related to the known oplopanane-4,10*α*-diol [31]. The difference was a 2-hydroxypropan-2-yl (δ_C 72.4, 31.9, 24.5, δ_H 1.09, s, δ_H 1.02, s) in **25** at C-7 replaced an isopropyl, which was confirmed by HMBC correlations between H_3-12 (δ_H 1.02) and C-7 (δ_C 55.5), C-11 (δ_C 72.4), between H_3-13 (δ_H 1.09) and C-7 (δ_C 55.5), C-11 (δ_C 72.4). The large coupling constants of H-5 (δ_H 2.00, brt, $J=9.0$ Hz), H-6 (δ_H 1.37, td, $J=10.9$, 8.0 Hz), and H-7 (δ_H 1.18, ddd, $J=13.3$, 10.5, 3.0 Hz) indicated the both *trans* configurations of H-5/H-6, H-6/H-7. In addition, the *trans* configuration of H-1/H-6 also could be deduced from the peak shape and coupling constants of H-6 (δ_H 1.37, td, $J=10.9$, 8.0 Hz). The relative configuration of **25** was further determined by NOE correlations observed from H-5 (δ_H 2.00) to H-7 (δ_H 1.18) and H-1 (δ_H 1.26), from H-6 (δ_H 1.37) to H_3-14 (δ_H 0.98) and H-4 (δ_H 4.23) (Fig. 3). Furthermore, comparing the ^{13}C NMR data of C-14 (δ_C 20.6) with that of oplopanone (δ_C 20.3) or 10-*epi*-oplopanone (δ_C 28.2) further confirmed above inference [31, 32]. Thus, the structure of **25** was identified as 4,10*α*,11-oplopananetriol and the configuration of C-4 undetermined as the less amount.

The molecular formula of compound **26** was determined as $C_{15}H_{28}O_3$ based on HRESIMS and ^{13}C NMR data. The ^1H NMR data (Table 5) presented one oxygenated methine (δ_H 3.50), three singlet methyls (δ_H 1.22, 1.16, 1.05), one doublet methyl (δ_H 1.04), and three active hydrogens (δ_H 4.26, 4.24, 3.95). The ^{13}C NMR data (Table 4) of **26** displayed 15 carbon signals, which were assigned to three oxygen-bearing carbons (δ_C 78.8, 72.9, 67.1), four methines (δ_C 52.0, 36.3, 23.8, 23.1), four methylenes (δ_C 39.4, 37.2, 27.6, 26.2), and four methyls (δ_C 30.6, 26.5, 26.4, 24.2) with the aid of HSQC experiment. The obviously upfield of H-6 (δ_H 0.13, dt, $J=10.3$, 3.4 Hz) and H-7 (δ_H 0.57, ddd, $J=10.0$, 8.0, 3.5 Hz) hinted **26** was a pallenane and related to 3*β*,4*β*-dihydroxypallenone [33, 34]. The C5/C3 bicyclic skeleton of **26** was established by ^1H–^1H COSY correlations between H-1/H-2/H-3, between H-1/H-6, H-1/H-5, and H-5/H-6. Furthermore, the ^1H–^1H COSY correlations from H-6/H-7/H-8/H-9/H-10/H_3-14 and H-10/10-OH revealed a 4-hydroxypentyl were connected with C-6. HMBC correlations from H-12 (δ_H 1.05) to C-7 (δ_C 52.0), C-11 (δ_C 72.9), from H-13 (δ_H 1.16) to C-7 (δ_C 52.0), C-11 (δ_C 72.9) elucidated a 2-hydroxypropan-2-yl was connected with C-7. Moreover, HMBC correlations from H-3 (δ_H 1.34) to C-4 (δ_C 78.8), C-5 (δ_C 36.3), from H-6 (δ_H 0.13) to C-2 (δ_C 26.2) and C-4 (δ_C 78.8), from H-7 (δ_H 0.57) to C-6 (δ_C 23.1), C-8 (δ_C 27.6), C-9 (δ_C 39.4), and C-11 (δ_C 72.9), from H_3-15 (δ_H 1.22) to C-3 (δ_C 37.2), C-4 (δ_C 78.8), C-5 (δ_C 36.3) further confirmed the planar structure (Fig. 2A). Comparing the ^1H NMR data of H-5 (δ_H 1.13, dd, $J=6.0$, 3.6 Hz), H-6 (δ_H 0.13, dt, $J=10.3$, 3.4 Hz), and H-7 (δ_H 0.57, ddd, $J=10.0$, 8.0, 3.5 Hz) with those of 3*β*,4*β*-dihydroxypallenone [33, 34] indicated **26** possessed the same H-1/H-5 *cis*, H-1/H-6 *trans*, H-5/H-6 *trans* configurations. This conclusion was confirmed by NOE correlations observed from H-7 (δ_H 0.57) to H-1

(δ_H 1.04) and H-5 (δ_H 1.13) (Fig. 3). The methyl at C-4 was determined as β deduced from NOE correlations observed from H-6 (δ_H 0.13) to H_3-15 (δ_H 1.22), from H-5 (δ_H 1.13) to 4-OH (δ_H 4.24). As there were potential inaccuracies of NOE correlations as the overlapped signals of H-1 and H_3-14. 1D and 2D NMR spectra of **26** were remeasured in pyridine-d_5 to get the distinct signals of H-1, H-5, H-6 and analysis of NOE correlations (in pyridine-d_5) further confirmed the configurations (Table S1, Additional file 1). Due to the configuration of methyl at C-4 differed from the congeners, **26** was named as 4-*epi*-pallenane-4α,10,11-triol.

The characteristic ^{1}H and ^{13}C NMR data (Tables 4, 5) of **27** showed it was also a pallenane sesquiterpenoid. The NMR data of **27** were similar to those of **26**, except for the presence of one methine (δ_C 35.0) instead of one oxygenated quaternary carbon as well as a doublet methyl replaced a singlet methyl. ^{1}H–^{1}H COSY correlations from H-4 (δ_H 2.15) to H_3-15 (δ_H 0.99) combining with HMBC correlations between H_3-15 (δ_H 0.99) and C-3 (δ_C 30.2), C-4 (δ_C 35.0), C-5 (δ_C 30.1) confirmed the methyl was located at C-4. (Fig. 2A). The similar ^{1}H NMR data of H-5 (δ_H 1.12, dt, $J=6.3$, 3.5 Hz), H-6 (δ_H 0.27, dt, $J=10.3$, 3.3 Hz), and H-7 (δ_H 0.56, ddd, $J=10.6$, 7.8, 3.5 Hz) with those of **26** suggested they possessed the identical configurations. In NOESY spectrum, the key cross peaks from H-6 (δ_H 0.27) to H_3-15 (δ_H 0.99), from H-4 (δ_H 2.15) to H-5 (δ_H 1.12), from H-7 (δ_H 0.56) to H-1 (δ_H 0.97) and H-5 (δ_H 1.12) further indicated that H-1, H-4, H-5, and H-7 were α-oriented, while H-6, and H_3-15 were β-oriented (Fig. 3). Finally, the structure of compound **27** was confirmed. Pallenane is a kind of rarely reported sesquiterpene with a distinctive C5/C3 bicyclic skeleton. Till now, only two pallenane congeners (3β,4β-dihydroxypallenone and 3β-acetoxy-4β-hydroxypallenone) were found from the plant *Pallenis spinosa* [33, 34]. The current compounds **26** and **27** were firstly obtained from streptomycete. According to the literature [33, 34], the isodaucane (**17**), oplopanane (**25**), and pallenane (**26**, **27**) skeleton metabolites were derived from the pinacol-type cadinane glycols through Wagner rearrangement in organisms (Fig. 2B). The 2-hydroxypropan-2-yl groups at C-7 in **26** and **27** were suggested as β-orientation according to the biogenetic way.

The characteristic ^{1}H and ^{13}C NMR signals implied that **28** was an eudesmane-type sesquiterpene and related to eudesmane-1β,6α,11-triol (**29**) [10]. The alterations were one more oxygenated methine replaced a methylene and a double bond replaced two methines. The HMBC correlations from H-4 (δ_H 2.39), H-7 (δ_H 2.02) to C-5 (δ_C 145.9) and H-4 (δ_H 2.39), H-7 (δ_H 2.02) to C-6 (δ_C 126.6) indicated double bond was located at C-5 and C-6, from 3-OH (δ_H 4.50) to C-2 (δ_C 35.6) and C-3 (δ_C 68.7) demonstrated an extra hydroxy was connected with C-3 (Fig. 2A). The relative configuration was determined by analysis of coupling constants and NOE correlations. The large coupling constants of H-1 (δ_H 3.03, dt, $J=11.6$, 4.8 Hz), H-3 (δ_H 3.52, m) and H-7 (δ_H 2.02, ddd, $J=11.0$, 6.2, 2.0 Hz) suggested that H-1, H-3, H-7 were axial orientation. While the peak shape and coupling constants of H-4 (δ_H 2.39, quint, $J=7.0$ Hz) suggested H-4 was equatorial orientation. NOE interactions from H-3 (δ_H 3.52) to H-4 (δ_H 2.39), H-1 (δ_H 3.03), from H-6 (δ_H 5.53) to H-4 (δ_H 2.39), H-7 (δ_H 2.02), from H_3-14 (δ_H 0.95) to 1-OH (δ_H 4.45) demonstrated that H-1, H-3, H-4, and H-7 were α-oriented, while 1-OH, 3-OH, H_3-14, and H_3-15 were β-oriented (Fig. 3). The configurations of chiral carbons of **28** were identified as 1*R*,3*S*,4*R*,7*R*,10*R* by comparing the experimental ECD spectrum of **28** with calculated ECD spectrum (Fig. 4G). Hence, the structure of **28** was determined as (1*R*,3*S*,4*R*,7*R*,10*R*)-eudesm-5-ene-1,3,11-triol.

The twenty-one known compounds were identified as bacaryolane B (**5**) [19], bacaryolane C (**6**) [19], caryolane-1,7α-diol (**7**) [35], caryolane-1,9α-diol (**8**) [36], 6α,9α-dihydroxy-β-caryolanol (**9**) [37], 6β,9β-dihydroxy-β-caryolanol (**10**) [37], caryolane-1,6β,9α-triol (**11**) [10], bacaryolane A (**12**) [19], 1(10)*E*,5*E*-germacradiene-2,11-diol (**16**) [26], ganodermanol L (**19**) [28],

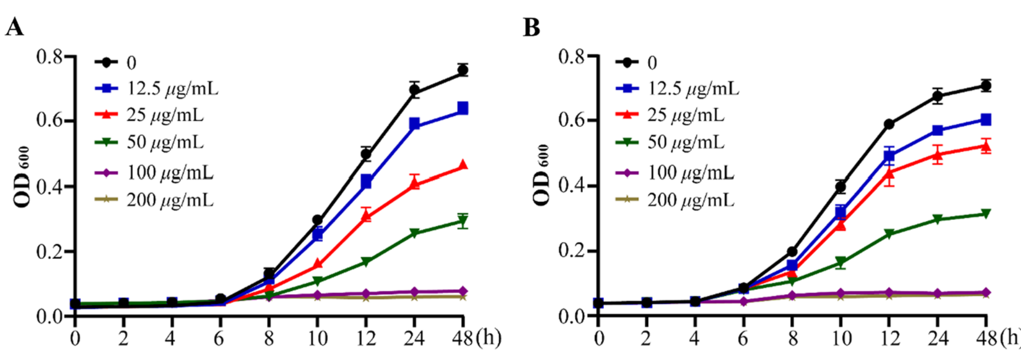

Fig. 5 The growth curve of **34** against *C. neoformans* (**A**) and *C. gattii* (**B**). Data are presented as mean ± SD of three independent determinations

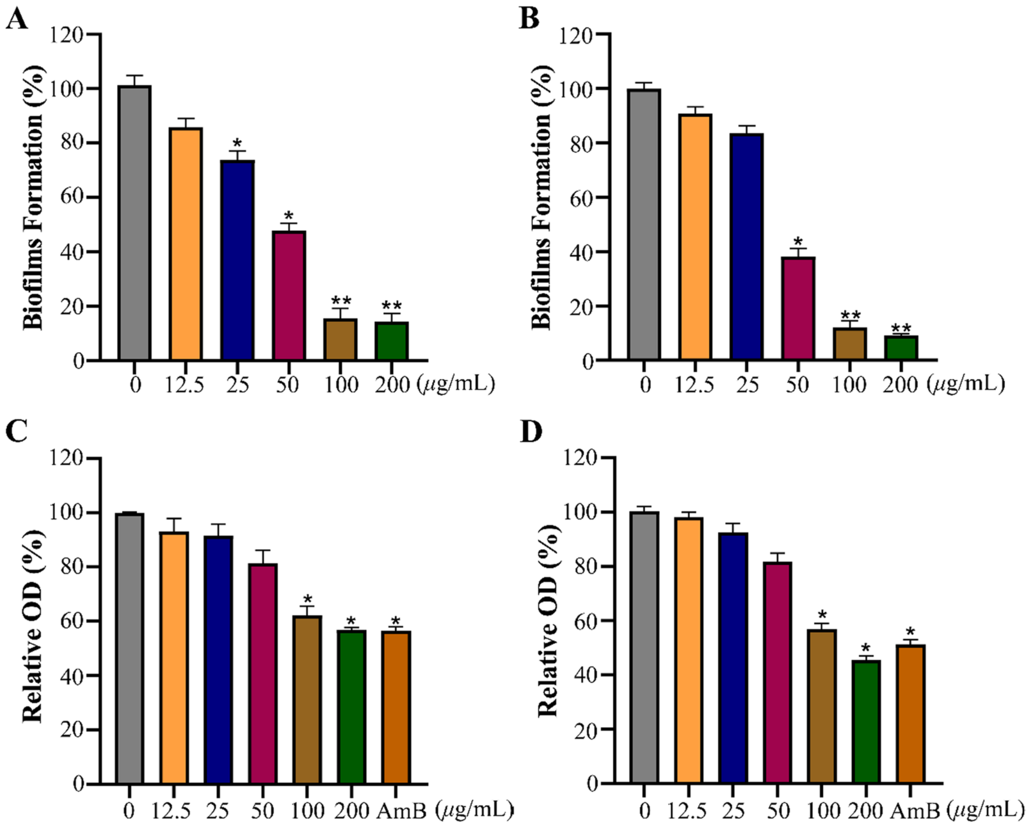

Fig. 6 The effect of **34** on the biofilm of *Cryptococcus* species. Effect of **34** on biofilm formation of *C. neoformans* (**A**) and *C. gattii* (**B**). Effect of **34** on the preformed biofilms of *C. neoformans* (**C**) and *C. gattii* (**D**). 2 μg/mL AMB was used as positive control. Data are presented as mean ± SD of three independent determinations. *$P < 0.05$, **$P < 0.01$ vs. control group

(1*α*,4*β*,5*β*,6*β*,7*β*,10*α*)-5,11-epoxy-10-cadinanol (**20**) [10], 15-hydroxy-*α*-cadinol (**21**) [29], pubinernoid C (**24**) [38], eudesmane-1*β*,6*α*,11-triol (**29**) [10], eudesmane-1*β*,6*α*,9*β*,11-tetrol (**30**) [10], ganodermanol J (**31**) [39], eudesmane-1*β*,5*α*,11-triol (**32**) [10], (2*α*,4*β*,5*β*,7*β*,10*α*)-2,5,11-eudesmanetriol (**33**) [10], *ent*-4(15)-eudesmene-1*β*,6*α*-diol (**34**) [40], 1*β*,6*α*-dihydroxy-4*β*(15)-epoxyeudesmane (**35**) [41] and 4*α*,15-epoxyeudesmane-1*β*,6*α*,11-triol (**36**) [28] by comparing their spectroscopic data with those reported in the literatures.

2.2 Evaluation of antimicrobial activity in vitro

The isolated sesquiterpenoids which amounted to more than 3 mg were chosen to evaluate their antimicrobial activities against five bacteria and four fungi. As presented in Table S2, Additional file 1, compounds **5–7**, **9**, **12**, **31–34** inhibited the growth against *C. albicans* and *C. parapsilosis* with the MIC_{80} values ranged from 100 to 400 μg/mL. Furthermore, **34** exhibited moderate antifungal activity against *C. neoformans* and *C. gattii* with MIC values of 50 μg/mL. The caryolane sesquiterpenoids **5–7** exhibited weak antibacterial activity against *B. subtilis*, *E. faecium*, and *E. coli* with MIC values ranged from 100–200 μg/mL, respectively (Table S3, Additional file 1). Meanwhile, the other tested compounds (**10**, **11**, **13**, **16**, **19–21**, **23**, **29**, **30**, **35**, **36**) didn't exhibit antimicrobial activity against test microorganisms at a concentration of 400 μg/mL.

2.3 34 inhibited *Cryptococcus* species in vitro

The optimal antifungal activity of **34** prompted us to further investigation its effect on *Cryptococcus* species. As shown in Fig. 5A, B, 34 consistently suppressed the growth of *Cryptococcus* species cells at all tested time points. Notably, at a concentration of 100 μg/mL, **34** could effectively eliminate almost all *Cryptococcus* species fungi. The above data demonstrated that **34** significantly inhibited the growth of *Cryptococcus* species in a time- and dose-dependent manner.

2.4 Effect of 34 on biofilm

The majority of fungal infections are attributed to biofilm, so inhibiting biofilm formation is crucial for effective

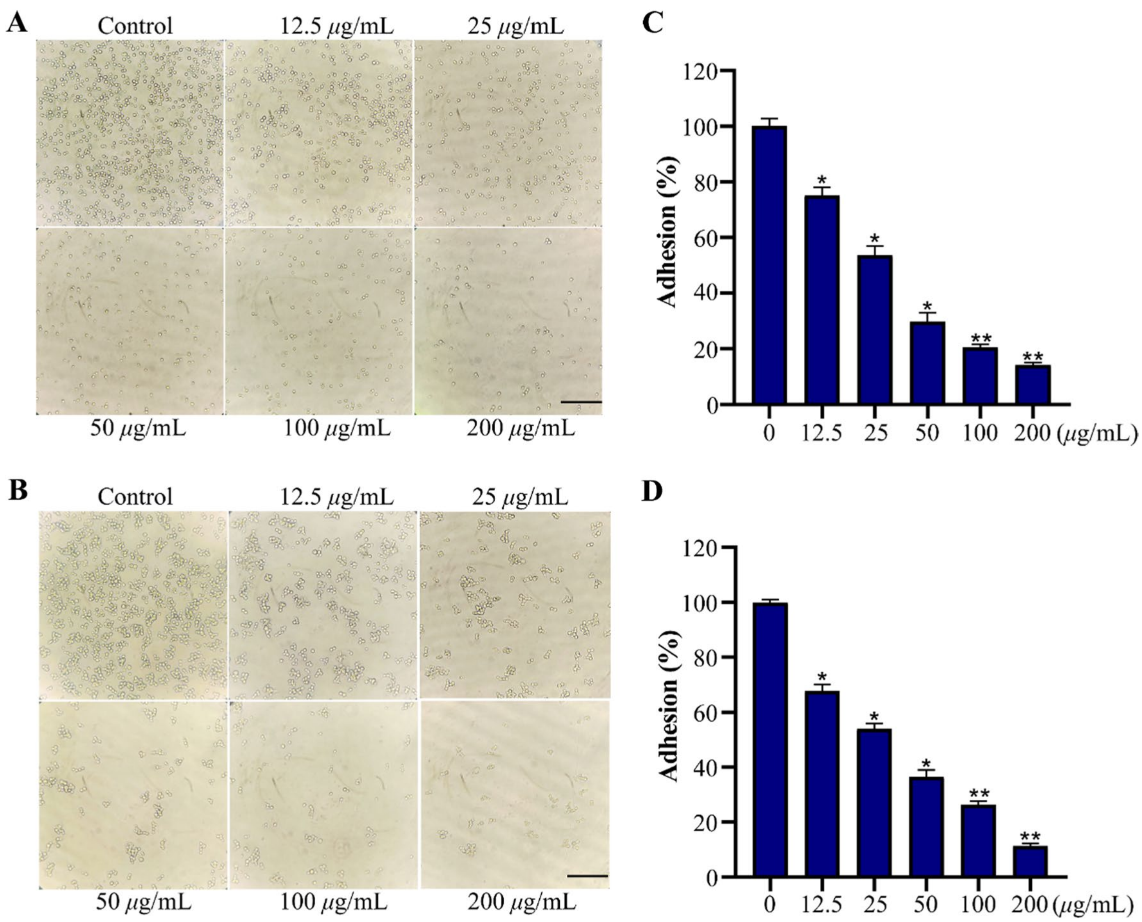

Fig. 7 The effect of **34** on *Cryptococcus* species adhesion. The photographs of *C. neoformans* cells (**A**) and *C. gattii* cells (**B**) treated with **34** for 4 h at 37 °C; The adhesion rates of *C. neoformans* cells (**C**) and *C. gattii* cells (**D**) was measured by XTT reduction assay. The bar in panel (**A**, **B**) indicates 40 μm. Data are presented as mean ± SD of three independent determinations. $^*P < 0.05$, $^{**}P < 0.01$ vs. control group

antifungal treatment [42]. Thereafter, the effect of **34** was further investigated on biofilm formation and preformed biofilm of *Cryptococcus* species. As displayed in Fig. 6A, B, the formation rate of biofilms for *C. neoformans* and *C. gattii* were decreased to 47.8% and 38.3%, respectively, at a dose of 50 μg/mL. As shown in Fig. 6C, D, 34 effectively destroyed the preformed biofilms of *Cryptococcus* species at a concentration of 100 μg/mL. These results indicated that **34** could not only inhibit biofilm formation, but also destroy preformed biofilms, which has the potential source for discovering novel therapeutic agents for treatment of fungal diseases.

2.5 34 inhibited the adhesion of *Cryptococcus* species

Adhesion is the initial step in host colonization and dissemination [43]. **34** was further evaluated for its ability to inhibit the adhesion of *Cryptococcus* species. Following treatment with various concentrations of **34**, the number of adherent *Cryptococcus* sp. cells exhibited a dose-dependent reduction trend compared to the untreated group (Fig. 7A, B). The above observation was further confirmed by the results of the XTT reduction assay. As shown in Fig. 7C, D, the adhesion rates for *C. neoformans* and *C. gattii* significantly decreased from 75.2% to 14.1% and from 67.7% to 11.3%, respectively after treated with **34** (12.5 to 200 μg/mL).

3 Experimental procedures

3.1 General

Optical rotation was determined using an Anton Paar MCP200 automatic polarimeter (Graz, Austria). IR spectra were recorded with a Bruker Tensor 27 FT-IR spectrometer. A biologic MOS-450 spectra polarimeter (Biologic Science, Claix, France) was used to measured ECD spectra. NMR spectra were recorded on a Bruker Advance III-600 MHz spectrometer (Bruker, Rheinstetten, Germany). ESIMS were recorded on an Agilent 1290–6420 Triple Quadrupole LC-MS spectrometer (Santa Clara, CA, USA). HRESIMS experiments were conducted using a Bruker Micro TOF-Q mass spectrometer (Bruker Daltonics, Billerica, MA). Silica gel (100–200 mesh, 200–300 mesh, Qingdao Marine Chemical, Ltd., Qingdao, China), Sephadex LH-20 (GE Healthcare Biosciences AB, Uppsala, Sweden), YMC*GEL ODS-A (S-50 µm, 12 nm) (YMC Co., Ltd., Kyoto, Japan) were used for column chromatography. Mosher's reagents R-MTPA-Cl and S-MTPA-Cl were purchased from Sigma Aldrich (Shanghai) Trading Co., Ltd. XTT and antimicrobial assays were analyzed using a microplate reader (BioTek Synergy H1, BioTek Instruments, Inc., Vermont, USA). The images of cells were observed directly with a microscope (Olympus IX71, Olympus, Tokyo, Japan).

3.2 Microbial material

The producing organism was derived from fresh fecal samples excreted by healthy adult *E. maximus* living in Xishuangbanna National Nature Reserve, Xishuangbanna, Yunnan Province, China. The strain was identified to be *S. fulvorobeus* by Dr. Yi Jiang based on morphological characteristics and 16S rRNA gene sequences. The BLAST result showed that the sequence was most similar (99.89%) to the sequence of *S. fulvorobeus* (strain: NBRC 15897, GenBank accession no. AB184711). The strain (No. YIM 103582) was deposited at the Yunnan Institute of Microbiology, Yunnan University, China.

3.3 Fermentation, extraction, and isolation

The strain was inoculated to 100 mL seed medium consisting of 4 g/L yeast extract, 4 g/L glucose, 5 g/L malt extract, 1.0 mL of multiple vitamin solution, and 1.0 mL of trace element solution at a pH of 7.2 without adjustment. The flasks were cultured for 2 days at 28 °C on a rotary shaker at 160 rpm, followed by inoculation to fermentation medium (24 g/L soluble starch, 3 g/L beef extract, 1 g/L glucose, 3 g/ L peptone, 5 g/L yeast extract, 4 g/L $CaCO_3$, pH 7.0) with a 10% volume. The fermentation was incubated at 28 °C for 7 days on a rotary shaker at 160 rpm.

The completed fermentation culture (150 L) was centrifuged (4000 rpm, 5 min) to separate into supernatant and mycelium, and the supernatant was extracted with ethyl acetate three times and evaporated to yield a crude extract 60 g. The dried extract was subjected to a silica gel column chromatography eluting with a CH_2Cl_2-MeOH solvent system (from 100:1 to 30:1, 10:1, and finally 1:1) to yield five fractions Fr.1–5. Fraction 1 was subjected to Sephadex LH-20 chromatography (MeOH) to produce three subfractions Fr.1.1-Fr.1.3. Fr.1.3 was subjected to silica gel column chromatography (P. ether-EtOAc 10:1) to yield three subfractions Fr.1.3.1-Fr.1.3.9. Fr.1.3.3 was isolated through ODS column chromatography MeOH-H_2O (60:40) to yield compounds **5** (4.6 mg), **6** (3.0 mg), and **7** (14.3 mg). Fr.1.3.5 was purified by silica gel column chromatography (P. ether-EtOAc 7:1) to afford compound **12** (8.8 mg), **20** (26.7 mg), **25** (2.0 mg), and **35** (5.0 mg). Fraction 2 was subjected to Sephadex LH-20 chromatography (MeOH) to obtain three subfractions Fr.2.1-Fr.2.3. Fr.2.3 was separated by silica gel column chromatoraphy (P. ether-EtOAc 4:1), followed by eluting with MeOH-H_2O (40:60) using ODS column chromatography to afford compounds **8** (2.2 mg), **16** (4.0 mg), **34** (16.6 mg), and **36** (6.2 mg). Fraction 3 was subjected to silica gel column chromatography (CH_2Cl_2-MeOH 50:1) to yield seven subfractions Fr. 3.1-Fr. 3.7. Fr. 3.1was put on an ODS column and eluted with MeOH-H_2O (40:60) to yield three subfractions Fr. 3.1.1-Fr. 3.1.3. Compounds **2** (2.5 mg), **18** (2.3 mg), **19** (57.8 mg), **29** (23.3 mg), and compound **33** (16.0 mg) were obtained from Fr.3.1.1 through a silica gel column chromatography (P. ether-EtOAc 6:1). Fr.3.3 was subjected to ODS column chromatography, eluting with MeOH-H_2O (45:55) to yield nine subfractions Fr.3.3.1-Fr.3.3.9. Fr.3.3.3 was fractionated by silica gel column chromatography (CH_2Cl_2-MeOH 50:1) to give compounds **9** (4.0 mg), **11** (15.0 mg), and **26** (1.6 mg). Fr.3.3.4 was separated by silica gel column chromatography (P. ether-EtOAc 2:1), then further purified by silica gel column chromatography (CH_2Cl_2-MeOH 50:1) to give compounds **1** (2.8 mg), **15** (2.3 mg), **17** (2.6 mg), **30** (23.7 mg), and **31** (3.2 mg). Compounds **21** (6.2 mg) and **32** (5.8 mg) were obtained from Fr.3.3.5 through a silica gel column chromatography (CH_2Cl_2-MeOH 60:1). Similarly, compounds **13** (5.2 mg) and **14** (2.6 mg) were isolated from Fr. 3.3.7 through a silica gel column chromatography (CH_2Cl_2-MeOH 60:1). Fr. 3.3.9 was purified by silica gel column chromatography (P. ether-EtOAc 2:1) to afford compounds **22** (2.3 mg) and **24** (2.0 mg). Fr.3.5 was separated by ODS column chromatography and eluted with MeOH-H_2O (30:70) to yield six fractions Fr.3.5.1–3.5.6. Fr.3.5.2 was purified by silica gel column chromatography (EtOAc–MeOH 40:1) to afford compounds **3** (2.0 mg) and **4** (2.6 mg). Fr.3.5.4 was purified by silica gel column chromatography (CH_2Cl_2-MeOH 25:1) to afford compounds **10** (3.8 mg) and **27** (1.5 mg). Fr.3.5.5 was firstly subjected to silica gel column chromatography (CH_2Cl_2-MeOH 25:1), then purified by silica gel column chromatography (P. ether-EtOAc 2:1) to give compounds **23** (3.2 mg) and **28** (2.0 mg).

3.4 Spectroscopic data of compounds

3.4.1 (1S,2R,4S,5S,8R)-9-Oxocaryolane-1,13-diol (1)

Colorless oil; $[\alpha]_D^{20}+60.0$ (*c* 0.20, MeOH); IR (film) ν_{max} 3727, 3382, 2938, 2866, 1699, 1455, 1054, 1033, 1013 cm^{-1}; CD (0.5 mg/mL, MeOH) λ_{max} ($\Delta\varepsilon$) 202 (-0.48), 294 ($+2.04$) nm; ^1H and ^{13}C NMR see Tables 1 and 2; HRESIMS *m/z* 275.1623 $[M+Na]^+$ (calcd for $C_{15}H_{24}NaO_3^+$, 275.1618).

3.4.2 (1S,2R,4R,5S,8R)-Caryolane-1,14-diol (2)

Colorless oil; $[\alpha]_D^{20} - 53.0$ (*c* 0.30, MeOH); IR (film) ν_{max} 3726, 3347, 2926, 2867, 1456, 1053, 1033 cm^{-1}; ^1H and ^{13}C NMR see Tables 1 and 2; HRESIMS *m/z* 239.2021 $[M+H]^+$ (calcd for $C_{15}H_{27}O_2^+$, 239.2006).

3.4.3 (1S,2R,4R,5S,8R,9S)-Caryolane-1,9,14-triol (3)

Colorless oil; $[\alpha]_D^{20} - 40.5$ (*c* 0.20, MeOH); IR (film) ν_{max} 3355, 2940, 2865, 1457, 1055, 1033, 1018 cm^{-1}; ^1H and ^{13}C NMR see Tables 1 and 2; HRESIMS *m/z* 277.1780 $[M+Na]^+$ (calcd for $C_{15}H_{26}NaO_3^+$, 277.1774).

3.4.4 Caryolane-1,6α,10α-triol (4)

Colorless solid; $[\alpha]_D^{20} - 54.0$ (*c* 0.37, MeOH); IR (film) ν_{max} 3348, 2928, 2866, 1461, 1363, 1109, 1040, 1004 cm^{-1}; ^1H and ^{13}C NMR see Tables 1 and 2; HRESIMS *m/z* 277.1778 $[M+Na]^+$ (calcd for $C_{15}H_{26}NaO_3^+$, 277.1774).

3.4.5 (2S,4S,7S,8S)-1(10)E,5E-Germacradiene-2,8,11-triol (13)

Colorless oil; $[\alpha]_D^{20} - 80.5$ (*c* 0.20, MeOH); IR (film) ν_{max} 3315, 2968, 2930, 1668, 1382, 1046, 1010 cm^{-1}; CD (0.5 mg/mL, MeOH) λ_{max} ($\Delta \varepsilon$) 231 (−25.77) nm; ^1H and ^{13}C NMR see Tables 2 and 3; HRESIMS *m/z* 277.1780 $[M+Na]^+$ (calcd for $C_{15}H_{26}NaO_3^+$, 277.1774).

3.4.6 (2S,4S,7R)-1(10)E,5E-Germacradiene-2,11-diol 2-methyl ether (14)

Colorless oil; $[\alpha]_D^{20} - 112.2$ (*c* 0.50, MeOH); IR (film) ν_{max} 3728, 2970, 2930, 1447, 1381, 1088, 934 cm^{-1}; CD (0.5 mg/mL, MeOH) λ_{max} ($\Delta \varepsilon$) 225 (−9.42), 290 (+0.38) nm; ^1H and ^{13}C NMR see Tables 2 and 3; HRESIMS *m/z* 275.1986 $[M+Na]^+$ (calcd for $C_{16}H_{28}NaO_2^+$, 275.1982).

3.4.7 (2S,4R,7S,8S)-1(10)E,5E-Germacradiene-2,4,8,11-tetraol 2-acetate (15)

White powder; $[\alpha]_D^{20} - 120.5$ (*c* 0.20, MeOH); IR (film) ν_{max} 3348, 2973, 2929, 1730, 1373, 1244, 1022 cm^{-1}; CD (0.5 mg/mL, MeOH) λ_{max} ($\Delta \varepsilon$) 200 (+29.35), 231 (−9.42) nm; ^1H and ^{13}C NMR see Tables 2 and 3; HRESIMS *m/z* 335.1833 $[M+Na]^+$ (calcd for $C_{17}H_{28}NaO_5^+$, 335.1829).

3.4.8 (1α,3α,4β,5α,6α,7β,9β)-6,11-Epoxyisodaucane-3,9-diol (17)

White powder; $[\alpha]_D^{20} + 13.3$ (*c* 0.30, MeOH); IR (film) ν_{max} 3360, 2927, 2869, 1460, 1366, 1236, 1049, 1028 cm^{-1}; ^1H and ^{13}C NMR see Tables 3 and 4; HRESIMS *m/z* 277.1788 $[M+Na]^+$ (calcd for $C_{15}H_{26}NaO_3^+$, 277.1774).

3.4.9 8α-Hydroxyganodermanol L (18)

White powder; $[\alpha]_D^{20} - 40.6$ (*c* 0.20, MeOH); IR (film) ν_{max} 3355, 2966, 2927, 1461, 1379, 1172, 1046 cm^{-1}; ^1H and ^{13}C NMR see Tables 3 and 4; HRESIMS *m/z* 293.1729 $[M+Na]^+$ (calcd for $C_{15}H_{26}NaO_4^+$, 293.1723).

3.4.10 (1S,2S,6R,7S,10R)-Cadinane-2,10,15-triol (22)

Yellow oil; $[\alpha]_D^{20} - 40.2$ (*c* 0.30, MeOH); IR (film) ν_{max} 3312, 2959, 2932, 2871, 1462, 1378, 1125, 1069, 1016 cm^{-1}; CD (0.25 mg/mL, MeOH) λ_{max} ($\Delta \varepsilon$) 194 (+9.63), 217 (−9.01), 237 (+1.85) nm; ^1H and ^{13}C NMR see Tables 4 and 5; HRESIMS *m/z* 277.1777 $[M+Na]^+$ (calcd for $C_{15}H_{26}NaO_3^+$, 277.1774).

3.4.11 (1R,3S,6R,7S,9S,10R)-3,9-Dihydroxyepicubenol (23)

Yellow oil; $[\alpha]_D^{20} - 16.0$ (*c* 0.50, MeOH); IR (film) ν_{max} 3354, 2960, 2877, 1450, 1659, 1369, 1060, 1030, 1007 cm^{-1}; CD (0.25 mg/mL, MeOH) λ_{max} ($\Delta \varepsilon$) 191 (−29.60), 213 (−11.77), 234 (+2.98) nm; ^1H and ^{13}C NMR see Tables 4 and 5; HRESIMS *m/z* 277.1775 $[M+Na]^+$ (calcd for $C_{15}H_{26}NaO_3^+$, 277.1774).

3.4.12 Oplopanane-4,10α,11-triol (25)

White amorphous power; $[\alpha]_D^{20} - 50.0$ (*c* 0.24, MeOH); IR (film) ν_{max} 3331, 2925, 2862, 1597, 1454, 1261, 1069, 1014 cm^{-1}; ^1H and ^{13}C NMR see Tables 4 and 5; HRESIMS *m/z* 279.1937 $[M+Na]^+$ (calcd for $C_{15}H_{28}NaO_3^+$, 279.1931).

3.4.13 4-epi-Pallenane-4α,10,11-triol (26)

Colorless oil; $[\alpha]_D^{20} - 202.0$ (*c* 0.10, MeOH); IR (film) ν_{max} 3358, 2965, 2867, 1600, 1458, 1372, 1185, 1124, 1003 cm^{-1}; ^1H and ^{13}C NMR see Tables 4 and 5; HRESIMS *m/z* 279.1936 $[M+Na]^+$ (calcd for $C_{15}H_{28}NaO_3^+$, 279.1931).

3.4.14 4-epi-Pallenane-10,11-diol (27)

Colorless oil; $[\alpha]_D^{20} - 80.6$ (*c* 0.20, MeOH); IR (film) ν_{max} 3349, 2927, 2865, 1602, 1457, 1372, 1126, 1082 cm^{-1}; ^1H and ^{13}C NMR see Tables 4 and 5; HRESIMS *m/z* 223.2039 $[M-H_2O+H]^+$ (calcd for $C_{15}H_{27}O^+$, 223.2056).

3.4.15 (1R,3S,4R,7R,10R)-Eudesm-5-ene-1,3,11-triol (28)

Colorless oil; $[\alpha]_D^{20} - 40.4$ (*c* 0.20, MeOH); IR (film) ν_{max} 3350, 2971, 2936, 1659, 1468, 1376, 1145, 1066, 1007 cm^{-1}; CD (0.5 mg/mL, MeOH) λ_{max} ($\Delta\varepsilon$) 206 (−16.93), 229 (+0.46) nm; ^{1}H and ^{13}C NMR see Tables 4 and 5; HRESIMS *m/z* 277.1779 $[M+Na]^+$ (calcd for $C_{15}H_{26}NaO_3^+$, 277.1774).

3.5 Esterification using Mosher's reagent

The 1 mg sample of compound **1** was dissolved in 0.5 mL of pyridine-d_5 and subsequently transferred into a pristine NMR tube. Then, the solution was subjected to treatment with (*R*)-MTPA-Cl (5 μL) for 12 h to obtained (*S*)-MTPA ester of **1** (**1a**). The (*R*)-MTPA ester of **1** (**1b**) was prepared by the same process. Subsequently, the tubes were directly employed for ^{1}H-NMR measurements. The (*S*)-MTPA esters (**2a** and **3a**) as well as (*R*)-MTPA esters (**2b** and **3b**) of compounds **2** and **3** were prepared in a completely analog manner.

3.6 ECD calculations

The ECD calculations of compounds **1**, **13–15**, **22**, **23**, and **28** were performed with Gaussian 09 [44]. The CONFLEX software was used to perform a stable conformational analysis of all enantiomers, employing the MMFF94S molecular force field and an energy cut off of 3 kcal/mol. The selected stable conformers were further optimized using the Gaussian 09 program package at the B3LYP/6-31G+(d) level of theory. Then, the ECD was theoretically calculated at the B3LYP/6-311 g++(2d, p) level in a methanol solution using the PCM model. SpecDis 1.51 software was used to generate the global theoretical ECD curve based on the Boltzmann weights of each conformer.

3.7 Antimicrobial assay

The antimicrobial activities were evaluated using a microbroth dilution method to determine the minimum inhibitory concentrations (MICs) [9]. The tested strains included five bacteria (*Bacillus subtilis* ATCC 6633, *Staphylococcus aureus* ATCC 25923, *Enterococcus faecium* ATCC19434, *Escherichia coli* ATCC 25922, *Pseudomonas aeruginosa* ATCC27853), as well as four fungi (*Candida albicans* ATCC MYA-2867, *C. parapsilosis* ATCC 22019, and *Cryptococcus neoformans* ATCC 208821, *C. gattii* CGMCC 2.3159). Antibacterial and antifungal tests were performed in Luria–Bertani and RPMI-1640 broth, respectively. Test compounds were dissolved in DMSO and twofold serially diluted to six different concentrations (40.0–1.25 mg/mL). Each well of the 96-well microtiter plates was added with 1 μL of test sample solutions and 100 μL of suspensions, which contained a concentration of 1×10^6 cfu/mL for bacteria (2×10^3 cfu/mL for fungi). The plates were subsequently incubated for 24 h at 28 °C for bacteria, 48 h at 28 °C for fungi. The XTT reduction assay was performed as described in the literature [45] and the absorbance at 490 nm was measured using a microplate reader for each well. The MIC was defined as the minimum concentration of the antimicrobial agent that completely inhibited visual growth of a microorganism, while the MIC_{80} was defined as the minimum concentration of the antimicrobial agent that inhibited 80% of the visible growth of a microorganism. Ciprofloxacin and amphotericin B were used as positive controls against bacteria and fungi, respectively.

3.8 Growth curve assay

The growth curve of *Cryptococcus* species was conducted according to the previously described method [45]. Briefly, the fungal suspensions were normalized to in the YPD liquid medium. Then, 100 μL fungal suspensions (1×10^6 cfu/mL) and different concentrations of compound **34** were inoculated into 96-well plate. The final concentrations of **34** were 12.5, 25, 50, 100 or 200 μg/mL. After incubating for 2, 4, 6, 8, 10, 12 and 24 h at 37 °C, the absorbance at 600 nm was determined by microplate reader (BioTek Synergy H1, BioTek Instruments, Inc., Vermont, USA).

3.9 Biofilm formation assay

The strains *C. neoformans* and *C. gattii* were selected to investigate the anti-biofilm activity of compound **34**. Biofilm formation was assessed by XTT reduction assay in 96-well plate [45]. Briefly, 100 μL of fungal suspensions (1×10^6 cfu/mL) were added to 96-well plates with varying different concentrations of **34** (12.5, 25, 50, 100 or 200 μg/mL). After incubation for 24 h at 30 °C, the plate was gently washed twice with sterile phosphate-buffered saline (PBS) to remove free-floating fungal cells. The biofilm of *Cryptococcus* species was assayed by XTT reduction assay.

3.10 Preformed biofilms assay

To evaluate the potential ability of compound **34** to disrupt preformed biofilms was assessed according to previously reported method [45]. 100 μL of fungal suspensions (1×10^6 cfu/mL) were dispensed into 96-well plate and cultured for 24 h at 37 °C. Then, the resulting preformed biofilm were washed twice with sterile PBS and treated with various concentrations of **34** (12.5, 25, 50, 100 or 200 μg/mL) or 2 μg/mL AMB. The plates were further incubated for 24 h, and then XTT reduction assay was conducted as described previously.

3.11 Adhesion assay

The impact of **34** on *Cryptococcus* species adhesion on 96-well plate was examined by XTT reduction assay according to a previously described method [45]. 100 µL suspensions of *C. neoformans* and *C. gattii* (1×10^6 cfu/mL) were respectively inoculated into 96-well plate, along with 1 µL of compound **34** at different concentrations (12.5, 25, 50, 100 or 200 µg/mL) and incubated at 37 °C for 4 h without shaking. Then, the cell supernatants were discarded and the plate was gently washed three times with sterile phosphate-buffered saline (PBS) to remove non-adherent cells. Then, the adherent *C. neoformans* and *C. gattii* were directly observed under a microscope in bright field mode and detected by XTT reduction assay.

4 Conclusion

In summary, we report the discovery of thirty-six structurally diverse sesquiterpenoids, including fifteen new compounds (**1–4**, **13–15**, **17**, **18**, **22**, **23**, **25–28**), along with twenty-one known analogues. These compounds featured eight distinctive carbon skeletons: caryolane, germacrane, cadinane, epicubenol, isaodaucane, oplopanane, pallenane, and eudesmane. It has been proven that *Streptomyces* possesses unparalleled ability to produce structurally diverse and novel secondary metabolites. Notably, parenane is a rare sesquiterpene with a unique C5/C3 bicyclic skeleton, which was first discovered in microorganisms. To our knowledge, *S. fulvorobeus* is the first actinomycete to produce such a substantial quantity of sesquiterpenoids. Additionally, the isolated sesquiterpenoid **34** exhibited optimal antifungal activity against *C. neoformans* and *C. gattii* with MIC values of 50 µg/mL. Further experiments showed that **34** significantly inhibited biofilm formation, destroyed the preformed biofilm of fungi, and prevented adhesion of *Cryptococcus* species. This work not only enriches the structural diversity of bacterial terpenoids but also provides support for the genetic capacity of actinomycetes to synthesize a diverse array of terpenoids.

Supplementary Information

The online version contains supplementary material available at https://doi.org/10.1007/s13659-024-00481-9.

Additional file 1: The antimicrobial activity of some compounds, HRESIMS, 1D and 2D NMR spectra of new compounds **1–4**, **13–15**, **17**, **18**, **22**, **23**, **25–28**, experimental ECD spectra and calculated ECD spectra of compound **12**.

Acknowledgements

This work was supported by National Natural Science Foundation of China (Grant No. 32060001), the Fundamental Research Funds for the Central Universities, China (No. N2320001) and the Construction Project of Liaoning Provincial Key Laboratory, China (2022JH13/10200026).

Author contributions

Lu Cao: investigation, writing of original draft. Jun-Feng Tan: conceptualization, methodology. Zeng-Guang Zhang and Jun-Wei Yang: methodology, data curation. Yu Mu and Zhi-Long Zhao: Investigation, data analysis. Yi Jiang: resources, and funding acquisition. Xue-Shi Huang and Li Han: revised the manuscript, supervision, and funding acquisition. All authors read and approved the final manuscript.

Availability of data and materials

Data will be made available on request.

Declarations

Competing interests

The authors declare no competing interests.

Author details

[1]Institute of Microbial Pharmaceuticals, College of Life and Health Sciences, Northeastern University, Shenyang 110819, China. [2]Pharmacological Laboratory, Liaoning Provincial Institute of Drug Inspection and Testing, Shenyang 110036, China. [3]Yunnan Institute of Microbiology, Yunnan University, Kunming 650091, China.

Received: 2 September 2024 Accepted: 8 October 2024
Published online: 02 December 2024

References

1. Tremaroli V, Bäckhed F. Functional interactions between the gut microbiota and host metabolism. Nature. 2012;489(7415):242–9.
2. Bartolini I, Risaliti M, Ringressi MN, Melli F, Nannini G, Amedei A, Muiesan P, Taddei A. Role of gut microbiota-immunity axis in patients undergoing surgery for colorectal cancer: focus on short and long-term outcomes. World J Gastroenterol. 2020;26(20):2498–513.
3. Ma J, Piao X, Mahfuz S, Long S, Wang J. The interaction among gut microbes, the intestinal barrier and short chain fatty acids. Anim Nutr. 2022;9:159–74.
4. Rakoff-Nahoum S, Paglino J, Eslami-Varzaneh F, Edberg S, Medzhitov R. Recognition of commensal microflora by toll-like receptors is required for intestinal homeostasis. Cell. 2004;118(2):229–41.
5. Bäckhed F, Ding H, Wang T, Hooper LV, Koh GY, Nagy A, Semenkovich CF, Gordon JI. The gut microbiota as an environmental factor that regulates fat storage. Proc Natl Acad Sci USA. 2004;101(44):15718–23.
6. Noverr MC, Huffnagle GB. Does the microbiota regulate immune responses outside the gut? Trends Microbiol. 2004;12(12):562–8.
7. Wu C, Chen T, Xu W, Zhang T, Pei Y, Yang Y, Zhang F, Guo H, Wang Q, Wang L, Zhao B. The maintenance of microbial community in human fecal samples by a cost effective preservation buffer. Sci Rep. 2021;11(1):13453.
8. Chen X, Li QY, Li GD, Xu FJ, Han L, Jiang Y, Huang XS, Jiang CL. The distal gut bacterial community of some primates and carnivora. Curr Microbiol. 2018;75(2):213–22.
9. Ding N, Jiang Y, Han L, Chen X, Ma J, Qu X, Mu Y, Liu J, Li L, Jiang C, Huang X. Bafilomycins and odoriferous sesquiterpenoids from *Streptomyces albolongus* isolated from *Elephas maximus* feces. J Nat Prod. 2016;79(4):799–805.
10. Ding N, Han L, Jiang Y, Li G, Liu J, Mu Y, Huang X. Sesquiterpenoids from *Streptomyces anulatus* isolated from *Giraffa camelopardalis* feces. Magn Reson Chem. 2018;56(5):352–9.
11. Zhang J, Jiang Y, Cao Y, Liu J, Zheng D, Chen X, Han L, Jiang C, Huang X. Violapyrones A-G, α-pyrone derivatives from *Streptomyces violascens* isolated from *Hylobates hoolock* feces. J Nat Prod. 2013;76(11):2126–30.
12. Ma J, Lei H, Chen X, Bi X, Jiang Y, Han L, Huang X. New anti-inflammatory metabolites produced by *Streptomyces violaceoruber* isolated from *Equus burchelli* feces. J Antibiot. 2017;70(10):991–4.
13. Mu Y, Yu X, Zheng Z, Liu W, Li G, Liu J, Jiang Y, Han L, Huang X. New metabolites produced by *Streptomyces badius* isolated from *Giraffa camelopardalis* feces. Magn Reson Chem. 2019;57(12):1150–7.
14. Zheng D, Han L, Qu X, Chen X, Zhong J, Bi X, Liu J, Jiang Y, Jiang C, Huang X. Cytotoxic fusicoccane-type diterpenoids from *Streptomyces*

violascens isolated from *Ailuropoda melanoleuca* feces. J Nat Prod. 2017;80(4):837–44.
15. Zheng D, Ding N, Jiang Y, Zhang J, Ma J, Chen X, Liu J, Han L, Huang X. Albaflavenoid, a new tricyclic sesquiterpenoid from *Streptomyces violascens*. J Antibiot. 2016;69(10):773–5.
16. Dickschat JS. Bacterial terpene cyclases. Nat Prod Rep. 2016;33(1):87–110.
17. Wu QX, Shi YP, Jia ZJ. Eudesmane sesquiterpenoids from the Asteraceae family. Nat Prod Rep. 2006;23(5):699–734.
18. Rinkel J, Rabe P, Garbeva P, Dickschat JS. Lessons from 1,3-hydride shifts in sesquiterpene cyclizations. Angew Chem Int Ed Engl. 2016;55(43):13593–6.
19. Ding L, Goerls H, Dornblut K, Lin W, Maier A, Fiebig HH, Hertweck C. Bacaryolanes A–-C, rare bacterial caryolanes from a mangrove endophyte. J Nat Prod. 2015;78(12):2963–7.
20. Chen S, Yang Q, Zhang X, Wang Z, Xu HM, Dong LB. Discovery of diverse sesquiterpenoids from *Crossiella cryophila* through genome mining and NMR tracking. J Nat Prod. 2024;87(2):195–206.
21. Yamada Y, Kuzuyama T, Komatsu M, Shin-Ya K, Omura S, Cane DE, Ikeda H. Terpene synthases are widely distributed in bacteria. Proc Natl Acad Sci USA. 2015;112(3):857–62.
22. Citron CA, Gleitzmann J, Laurenzano G, Pukall R, Dickschat JS. Terpenoids are widespread in actinomycetes: a correlation of secondary metabolism and genome data. ChemBioChem. 2012;13(2):202–14.
23. Rudolf JD, Alsup TA, Xu B, Li Z. Bacterial terpenome. Nat Prod Rep. 2021;38(5):905–80.
24. Tsuda M, Toriyabe Y, Endo T, Kobayashi J. Application of modified mosher's method for primary alcohols with a methyl group at C2 position. Chem Pharm Bull. 2003;51(4):448–51.
25. Nakano C, Horinouchi S, Ohnishi Y. Characterization of a novel sesquiterpene cyclase involved in (+)-caryolan-1-ol biosynthesis in *Streptomyces griseus*. J Biol Chem. 2011;286(32):27980–7.
26. Guan S, Grabley S, Groth I, Lin W, Christner A, Guo D, Sattler I. Structure determination of germacrane-type sesquiterpene alcohols from an endophyte *Streptomyces griseus* subsp. Magn Reson Chem. 2005;43(12):1028–31.
27. Kato R, Saito H, Ikeuchi K, Suzuki T, Tanino K. Total synthesis and structural revision of the 6,11-epoxyisodaucane natural sesquiterpene using an anionic 8π electrocyclic reaction. Org Lett. 2022;24(43):7939–43.
28. Lu S, Hu J, Xie X, Huang R, He J. Sesquiterpenoids isolated from feces-residing *Streptomyces* sp. inhibit the cellular entry of influenza a viruses. Nat Prod Res. 2022;36(24):6286–96.
29. Kuo YH, Chen CH, Chien SC, Lin YL. Five new cadinane-type sesquiterpenes from the heartwood of *Chamaecyparis obtusa* var. *formosana*. J Nat Prod. 2002;65(1):25–8.
30. Zhang Y, Jiang K, Zhai YM, Tan JJ, Meng DL, Guo SL, Qu SJ, Tan CH. Sesquiterpenoids and their glycosides from *Gynura procumbens*. Helv Chim Acta. 2014;97(3):369–74.
31. Yang JL, Zhao YM, Shi YP. Sesquiterpenoids from the rhizomes of *Homalomena occulta*. Nat Prod Bioprospect. 2016;6(4):211–6.
32. Piers E, Gavai AV. A (*Z*)-ethylidenecyclopentane annulation method. Total syntheses of (±)-anhydrooplopanone, (±)-oplopanone, and (±)-8-epi-oplopanone. J Org Chem. 1990;55(8):2380–90.
33. Ahmed AA, Jakupovic J, Bohlmann F. Dihydroxypallenone, a sesquiterpene with a new carbon skeletonerom pallenisspinosa. Phytochemistry. 1990;29(10):3355–8.
34. Appendino G, Jakupovic J, Jakupovic S. Sesquiterpenoids from *Pallenis spinosa*. Phytochemistry. 1997;46(6):1039–43.
35. Yang Z, Yang Y, Yang X, Zhang Y, Zhao L, Xu L, Ding Z. Sesquiterpenes from the secondary metabolites of *Streptomyces* sp. (YIM 56130). Chem Pharm Bull. 2011;59(11):1430–3.
36. Heymann H, Tezuka Y, Kikuchi T, Supriyatna S. Constituents of *Sindora sumatrana* MIQ. I. Isolation and NMR spectral analysis of sesquiterpenes from the dried pods. Chem Pharm Bull. 1994;42(1):138–46.
37. Chen QJ, Ouyang MA, Tan QW, Zhang ZK, Wu ZJ, Lin QY. Constituents from the seeds of *Brucea javanica* with inhibitory activity of *Tobacco mosaic virus*. J Asian Nat Prod Res. 2009;11(6):539–47.
38. Ding L, Görls H, Hertweck C. Plant-like cadinane sesquiterpenes from an actinobacterial mangrove endophyte. Magn Reson Chem. 2021;59(1):34–42.
39. Tan Z, Zhao J, Liu J, Zhang M, Chen R, Xie K, Dai J. Sesquiterpenoids from the cultured mycelia of *Ganoderma capense*. Fitoterapia. 2017;118:73–9.
40. Nagashima F, Kishi K, Hamada Y, Takaoka S, Asakawa Y. *ent*-Verticillane-type diterpenoids from the Japanese liverwort *Jackiella javanica*. Phytochemistry. 2005;66(14):1662–70.
41. Li X, Yang M, Han YF, Gao K. New sesquiterpenes from *Erigeron annus*. Planta Med. 2005;71(3):268–72.
42. Wu S, Wang Y, Liu N, Dong G, Sheng C. Tackling fungal resistance by biofilm inhibitors. J Med Chem. 2017;60(6):2193–211.
43. Forsyth CB, Mathews HL. Lymphocyte adhesion to *Candida albicans*. Infect Immun. 2002;70(2):517–27.
44. Xu W, Tan J, Mu Y, Zheng D, Huang X, Li L. New antimicrobial terpenoids and phloroglucinol glucosides from *Syzygium szemaoense*. Bioorg Chem. 2020;103:104242.
45. Tan J, Zhang Z, Zheng D, Mu Y, Cao B, Yang J, Han L, Huang X. Structure–activity relationship and biofilm formation-related gene targets of oleanolic acid-type saponins from *Pulsatilla chinensis* against *Candida albicans*. Bioorg Chem. 2024;146:107311.

Publisher's Note